




Review

Recent Progress in the Development of Composite Membranes Based on Polybenzimidazole for High Temperature Proton Exchange Membrane (PEM) Fuel Cell Applications

Jorge Escorihuela ^{1,*} , Jessica Olvera-Mancilla ², Larissa Alexandrova ² , L. Felipe del Castillo ² and Vicente Compañ ^{3,*} 

¹ Departamento de Química Orgánica, Universitat de València, Av. Vicent Andrés Estellés s/n, Burjassot, 46100 Valencia, Spain

² Departamento de Polímeros, Instituto de Investigaciones en Materiales, Universidad Nacional Autónoma de México (UNAM), Ciudad Universitaria, Coyoacán, Ciudad de México 04510, Mexico; olverajessica@iim.unam.mx (J.O.-M.); laz@unam.mx (L.A.); lfelipe@unam.mx (L.F.d.C.)

³ Departamento de Termodinámica Aplicada (ETSII), Universitat Politècnica de València, Camino de Vera. s/n, 46022 Valencia, Spain

* Correspondence: jorge.escorihuela@uv.es (J.E.); vicommo@ter.upv.es (V.C.); Tel.: +34-96-387-9328 (V.C.)

Received: 21 July 2020; Accepted: 17 August 2020; Published: 19 August 2020



Abstract: The rapid increasing of the population in combination with the emergence of new energy-consuming technologies has risen worldwide total energy consumption towards unprecedented values. Furthermore, fossil fuel reserves are running out very quickly and the polluting greenhouse gases emitted during their utilization need to be reduced. In this scenario, a few alternative energy sources have been proposed and, among these, proton exchange membrane (PEM) fuel cells are promising. Recently, polybenzimidazole-based polymers, featuring high chemical and thermal stability, in combination with fillers that can regulate the proton mobility, have attracted tremendous attention for their roles as PEMs in fuel cells. Recent advances in composite membranes based on polybenzimidazole (PBI) for high temperature PEM fuel cell applications are summarized and highlighted in this review. In addition, the challenges, future trends, and prospects of composite membranes based on PBI for solid electrolytes are also discussed.

Keywords: fuel cells; proton exchange membrane; polymer; polybenzimidazole; composite membranes; conductivity; carbon nanotubes; graphene oxide; ionic liquids; metal organic frameworks

1. Introduction

Proton conductivity has received intense attention owing to its application in chemical sensors, electrochemical devices, and power generation [1,2]. Proton conducting membranes form an important part in fuel cells (FCs), batteries, and supercapacitors [3]. Fuel cells based on proton exchange membranes (PEMs) are one of the most promising alternative energy sources because of their high efficiency, high power density, low emissions, and energy supply [4,5]. These alternatives provide the possibility of receiving energy from hydrogen, synthetic, or bio-synthetic fuels and can operate with greater efficiency and environmental sustainability compared with thermal motors [6,7]. Fuel cells can be used for a wide variety of technological devices such as vehicles, mobile phones, portable electronics, and power generators [8–10]; they are generally classified by the kind of electrolyte they use. Common classifications include alkaline fuel cells [11], direct methanol fuel cells [12], polymer electrolyte membrane fuel cells [13], phosphoric acid fuel cells [14], molten carbonate fuel cells [15], solid oxide fuel cells [16], and reversible fuel cells (also called unitized regenerative fuel cells) [17].

In a typical proton exchange membrane fuel cell (PEMFC), the polymer electrolyte membrane is responsible for proton conductivity, which allows the transport of protons from the anode to the cathode, constituting the essential component of the electrochemical device [18]. PEMFCs constitute a promising alternative to fossil fuels as they generate water as a byproduct and use only hydrogen and oxygen as reactants (Figure 1). According to their range of operating temperatures, PEMFCs can be classified into three main categories: (a) low temperature PEMFCs (LT-PEMFCs), which operate around 50–80 °C [19]; (b) intermediate temperature (IT-PEMFCs), which operate in the 80–120 °C range [20–22]; and (c) high temperature (HT-PEMFCs), which operate from 140 °C up to 200 °C [23,24], generally under anhydrous conditions. Among the numerous types of PEMs, membranes based on perfluorosulfonic acid polymers, such as Nafion[®] (Figure 2), have wide acceptance as they have been demonstrated to possess good conductivity as well as chemical and mechanical properties, have been used at temperatures below 90 °C, and have endured conditions of high relative humidity [25].

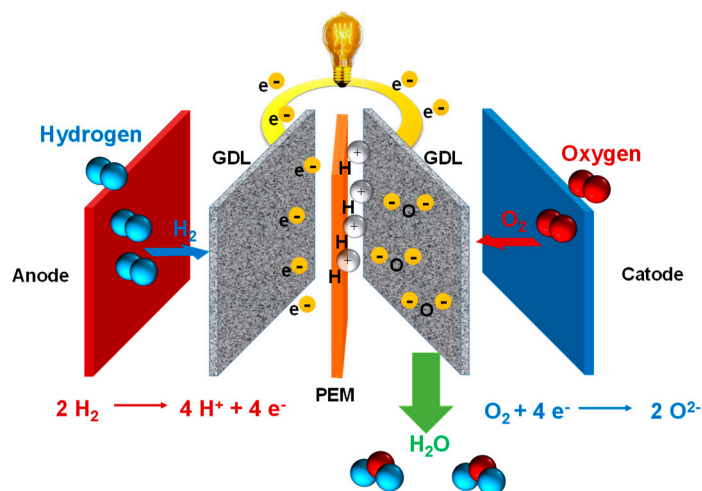


Figure 1. Schematic flow of PEMFC.

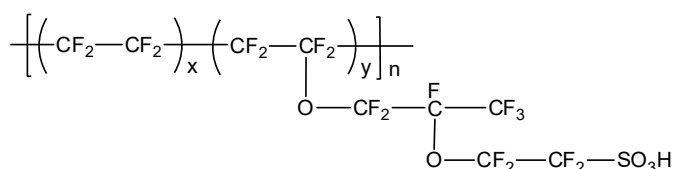


Figure 2. Chemical structure of Nafion[®].

Nafion[®], developed by DuPont in the late 1960s, still remains as the state-of-the-art membrane for low temperature PEMFCs (LT-PEMFCs). The main drawbacks of Nafion[®] membranes are mainly their costly manufacturing process, the destruction of the polymer structure at higher temperatures, and the strong decrease in proton conductivity at temperatures above 90 °C when low hydration conditions are reached [26–30]. Consequently, Nafion[®]-based membranes are limited to operate as LT-PEMFCs. These practical limitations have promoted the development of membranes that may be applied in HT-PEMFCs operating temperatures in the range of 140–200 °C and, hence, in the absence of water [31–35].

Among the benefits of working at high temperatures, it is worth mentioning a decrease in the catalyst contamination by CO and CO₂ poisoning, as the kinetics in the electrodes are faster and have a simpler thermal and water handling, low dependency on cooling systems, a high amount of reusable heat energy, as well as a lower cost of the membrane-electrode assemblies (MEAs) in comparison with LT-PEMFCs based on Nafion[®] [36–38]. The high CO tolerance of the anode catalyst makes it possible for an FC to use hydrogen directly from a simple methanol reformer, thus the selective oxidant and/or CO separator device can be removed from the processing system. Consequently,

the size of an FC is importantly reduced, improving its performance, responsiveness, and reliability, which ultimately allows to bring down system maintenance and operating costs [39]. In order to optimize the performance of FCs, a lot of work has been done in the development of HT-PEMs, particularly on those based on polybenzimidazoles (PBIs), which have emerged as promising candidates to operate at high temperatures [40–44].

PBIs are aromatic linear heterocyclic macromolecules that belong to the class of high performance polymers; they are highly resistant to acids and bases; have high glass transition temperatures (425–436 °C); and possess excellent thermal and mechanical stability, low flammability, and high energy radiation resistance. Aromatic polybenzimidazoles were firstly synthesized by H. Vogel and C. S. Marvel in 1961 [45], and as a consequence of their exceptional thermal and oxidative stability, they were used on aerospace and defense applications by NASA and the Air Force Materials Laboratory (AFML), respectively. The most widely studied polybenzimidazole is one commercialized by the corporation Celanese, poly [2,2'-(*m*-phenylene)-5,5'-bibenzimidazole], or *m*-PBI (also known as simply PBI). This polymer can be synthesized by a polycondensation reaction using 3,3'-diaminobenzidine (DAB) and isophthalic acid (IPA) [46,47]. Another available polybenzimidazole is poly (2,5-benzimidazole) (or AB-PBI), which was also carefully studied as membrane for HT-PEMFCs. The AB-PBI is prepared by condensation of 3,4-diaminobenzoic acid (DABA) [48]. The chemical structures of both *m*-PBI and AB-PBI are shown in Figure 3.

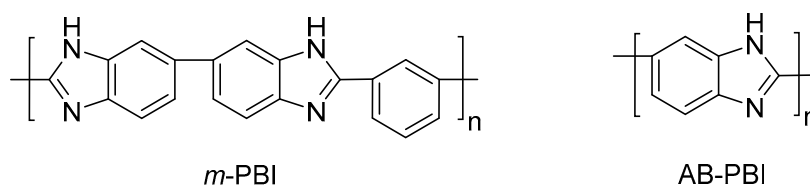


Figure 3. Chemical structures *m*-PBI and AB-PBI.

However, to achieve the high proton conductivity levels required for HT-PEMFCs, these simple PBIs need to be doped with acid because their intrinsic conductivity is very low (around 10^{-12} S/cm). In particular, phosphoric acid (PA)-doped PBI membranes demonstrated good thermal and mechanical stability, low gas permeability, and conductivity values between 0.07 and 0.2 S/cm at approximately 200 °C without any additional humidification [49,50]. As the ionic conductivity of PA is low at low temperatures, PBI embedded in PA operating temperature range is about 150–250 °C. The hydrogen oxidized at the anode splits into protons and electrons. The electrons pass through the external electrical circuit, whereas the protons are transferred through the electrolyte. On the cathode side, the redox reaction between positive hydrogen ions, electrons, and oxygen gas results in water formation [51]. The main advantage of phosphoric fuel cells is their capacity to generate and separate electricity and useful heat at the same time. However, the use of this acid-doping method presents various inconveniences, limiting the applications; particularly, the pyrolysis of PA above 190 °C [50], the migration of PA resulting in loss of transition metal catalyst and reducing proton conductivities, acid leaching problems, and reduced mechanical properties under HT-PEMFCs' operation conditions.

Another efficient method to increase conductivity is the introduction of the covalently bound sulfonic and/or phosphoric groups into the backbone chains, but multi-step complex syntheses are generally needed for the formation of such PBIs [52,53]. Additionally, the aggressive polymerization conditions may affect the side-groups, resulting in a crosslinked polymer gel instead of a linear structure. Consequently, the possible structural variations in the polymers are limited and PBIs containing functional groups in their main chain are scarce. PBIs obtained by changing one of the monomers allow for the modification of the physico-chemical properties (e.g., basicity), simply by playing with the number of the nitrogen atoms in the monomer and their distribution along the polymer [54]; in this manner, acid leaching can be minimized [55].

The doping strategies for PBI-type membranes consist of an incorporation of significant amounts of phosphoric acid to the polymer matrix to achieve sufficient proton conductivity. The acid doping can be performed in various ways. The simplest and most efficient method consists of directly immersing the PBI-type membrane sheet into hot phosphoric acid. The doping level of the membrane depends on the immersion time and temperature. As an example, the AB-PBI based-membrane doped at 120 °C for 24 h can absorb phosphoric acid up to 2.5 times its own weight, which corresponds to the chemical formula AB-PBI·5H₃PO₄. On the other hand, the thickness practically doubles during the doping process. For example, the thickness changed from 50 μm for a pristine PBI membrane to almost 100 μm when it was fully doped [56]. The interaction between acid and the polymer matrix occurs via the N-imidazole sites. The basic N-sites of PBI act as proton acceptors like in a standard acid–base reaction, creating the ion pairs in this process as shown in Figure 4. Therefore, the polymer bearing more basic N-sites forms stronger bonds with acids.

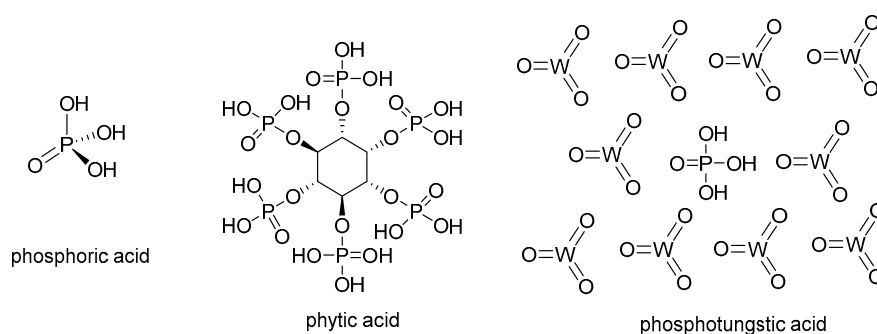


Figure 4. Chemical structures of phosphoric acid, phytic acid, and phosphotungstic acid.

The conductivity depends not only on the doping level, but also on the acid distribution within the membrane. In this sense, the membranes should ensure that the acid percolates throughout the polymer network and interacts with nearly every basic N-site of the polymer matrix. Finally, the conductivity of composite membranes based on PBIs is also affected by the dehydration reaction of phosphoric acid. It was noticed that, under anhydrous conditions, the conductivity of phosphoric acid decreases for temperatures above 140 °C owing to a condensation reaction of PA affording pyrophosphoric acid (H₄P₂O₇) and water. Therefore, at temperatures between 140 and 180 °C, the cell resistance of MEA based on PBIs under open circuit conditions is significantly higher than that with an electrical load and, additionally, it allows to produce water through the fuel cell reaction. The water formed permits the rehydration of the membrane in the MEA and results in a better conducting phosphoric acid [57].

Despite the wide use of PA as acid doping for PBI-based membranes, other acids have been used in the past years to overcome the drawbacks associated with the use of PA, mainly acid leaching and corrosion, which can seriously affect the long-term stability of fuel cells. Among other doping acids containing phosphonate groups, phytic acid (myo-inositol hexakisphosphate) is considered a sustainable alternative to phosphoric acid (Figure 4). Phytic acid is a phosphorus-containing organic acid that can be found in plants, especially in seeds and fibers. This acid has been used as a doping agent in combination with metal organic frameworks (MOFs) for polymer electrolyte membranes based on Nafion[®], reaching high proton conductivities [58,59]. Because of its molecular size, this natural acid can be encapsulated into cavities, reducing the leaching from the membrane. Another type of alternative acid is heteropolyacids, which are a particular class of acids made up of a combination of hydrogen and oxygen with metals and non-metals. Among this family of heteropolyacids, phosphotungstic acid (HPW), with molecular formula H₃P₄W₁₂O₄₀, has been efficiently applied as a proton carrier in proton exchange membrane fuel cells [60,61]. Some representative literature on heteropolyacid doped polymer as PEM should be consulted [62,63]. In a recent work, we have evaluated the long-term stability of PBI membranes doped with different concentrations of the widely used PA, and an important acid leaching and subsequent conductivity drop was observed [64].

2. Proton Conduction and Transport Mechanism

As has been previously commented, the proton conductivity of acid-doped PBI membranes is strongly dependent on the physico-chemical parameters such as temperature, relative humidity (RH), as well as the acid doping level measured in molar concentration of the doping solution [65,66]. Such conductivity is generally accepted to occur by two different mechanisms [67]: the Grotthuss mechanism (also known as hopping mechanism) and the vehicle mechanism. The prevalence of either the hopping or vehicle mechanism depends on the hydration level of the membrane. On the other hand, the mechanism of proton transport in composite and hybrid membranes is much more complex as it involves both the surface and chemical properties of the inorganic and organic phases present in the composite membrane.

The Grotthuss mechanism is characterized by the protons' jumping from one site to another along a hydrogen-bonding (HB) chain. In the case of PBI composite membranes, the protons are transferred from the nitrogen benzimidazole sites (N–H) to the phosphoric acid anions inside of the polymer matrix. This contribution is relevant for $n = [\text{H}_3\text{PO}_4]/[\text{PBI}] < 2$. When $n > 2$, there is a possibility of a proton hopping along the phosphoric acid anions. This mechanism is relevant in the case of non-doped PBI. The original idea was proposed by Theodore von Grotthuss in 1806 to explain a mechanism for proton (H^+) transport between water molecules [68]. As shown in Figure 5, the protons jump from a protonic species such as H_3O^+ to another protonic species in the membrane [69].

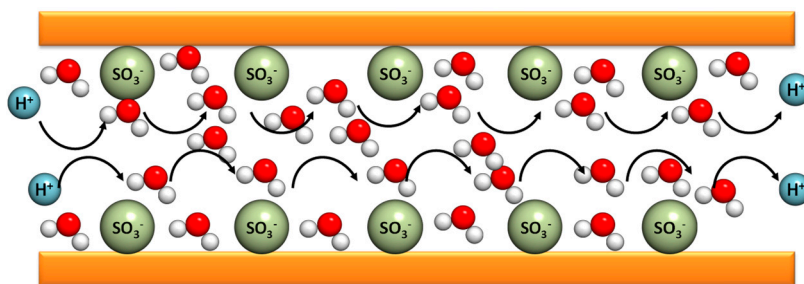


Figure 5. Schematic representation of the Grotthuss mechanism in a polymeric membrane.

The second mechanism, namely the vehicle mechanism, was proposed in 1982 by Kreuer, Rabenau, and Weppner [70] and rationalizes that the motion of protons is assisted by carrying molecules that, in general, are associated to the doping acidic groups. This last mechanism accounts for the major contribution for the conductivity increment of the polymeric membranes. Finally, a combination of the two described mechanisms can be observed in the case of diffusion of protons as part of polymeric structures involving molecules of water such as H_3O^+ , H_5O_2^+ (Zundel cation), H_9O_4^+ (Eigen cation), or some other species, such as NH_4^+ , which may also be present in the polyelectrolyte, in combination with the diffusion of vehicles as uncharged molecules. As illustrated in Figure 6, the protons attach themselves to a vehicle site such as water, which is diffused through the medium, and thus carry the protons along.

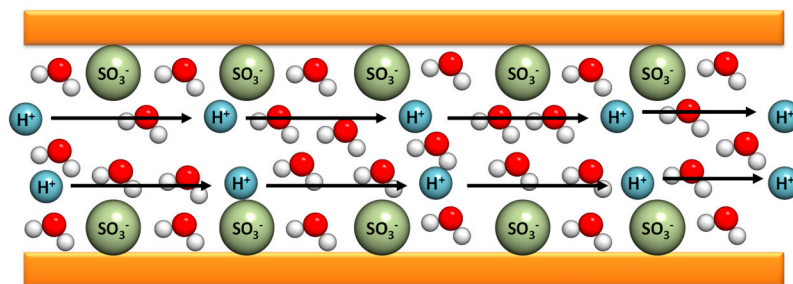


Figure 6. Schematic representation of the vehicular mechanism in a polymeric membrane.

When the protons are moving through a hopping mechanism, the conductivity of the acid-doped PBI is governed by an activation mechanism that obeys the Arrhenius law [71], where the relation between the conductivity and temperature is governed by the expression.

$$\sigma = A \exp\left(-\frac{E_a}{RT}\right), \quad (1)$$

where σ (S/cm) is the proton conductivity at a certain RH, A is a pre-factor, E_a (kJ/mol) is the activation energy at a certain RH, R (8.314 J/mol K) is the gas constant, and T (K) is the absolute temperature.

The values of E_a for $n > 2$ are in the range 15–25 kJ/mol, very near to that of concentrated H_3PO_4 aqueous solution. In this situation, PBI-based membranes doped with acidic groups show high proton conductivity if properly doped with strong acids such as H_3PO_4 depending on the amount of PA absorbed into the porous of its matrix. In fact, PBI is a basic polymer, which dissociates PA releasing protons, as sketched by the following reaction: $H_3PO_4 + PBI \rightarrow H_2PO_4^- + PBI^+H^+$, where the equilibrium constant is about $K = 1.17 \times 10^3$ and H^+ ions can migrate through the polymer backbone by means of hydrogen bonds, in this case, assisted by phosphate anions by means of the Grotthuss mechanism, as we previously mentioned.

In some cases, such as PA-doped composite membranes of PBI containing ionic liquids, the dependence of the conductivity versus temperature presents a different behavior than the typical Arrhenius behavior and the activation energy associated with the conductivity mechanism is not constant for the entire the range of temperatures. In such a situation, the conductivity of the membranes exhibits a Vogel–Tammann–Fulcher (VTF) conduction behavior, where proton hopping is coupled with the segmental motion of the polymer chains and the activation mechanism is given according to the equation.

$$\ln \sigma_{dc} = \ln \sigma_{\infty} - \frac{B}{T - T_0}, \quad (2)$$

where B is the fitting parameter related with the curvature of the experimental data plot; T_0 is the Vogel temperature, which is considered as the one at which the relaxation time would diverge; and σ_{∞} is the pre-factor related with the conductivity limit at high temperatures.

Figure 7 displays the results found for the conductivity of some composite membranes of PBI filled with ionic liquids (ILs), where a behavior different from linear is observed depending on the IL type. The activation energy associated with this kind of composite membrane is much higher for lower temperatures than the one associated with higher temperatures, in agreement with the experimental results. The values for the activation energy obtained from the fit of Equation (2) to the experimental data plotted in Figure 7 follow the trend $[Cl]^-$ (6.33 kJ/mol) > $[I]^-$ (5.80 kJ/mol) > $[NTf_2]^-$ (5.35 kJ/mol) > $[Br]^-$ (3.04 kJ/mol) > $[NCS]^-$ (2.91 kJ/mol) > $[BF_4]^-$ (2.53 kJ/mol) \approx $[PF_6]^-$ (2.51 kJ/mol). A close inspection of Figure 7 reveals a change in the slopes. For PBI@BMIM-NTf2 and PBI@BMIM-Cl, a negative slope is observed at high temperatures, in contrast with a slightly positive slope for PBI@BMIM-NCS and PBI@BMIM-BF4. This behavior can be associated with the variation in Debye's length, which is related to the effective dissociation energy and the measured dielectric permittivity in the absence of electrode polarization as well as of orientational polarization of dipolar ions, as previously reported [72,73].

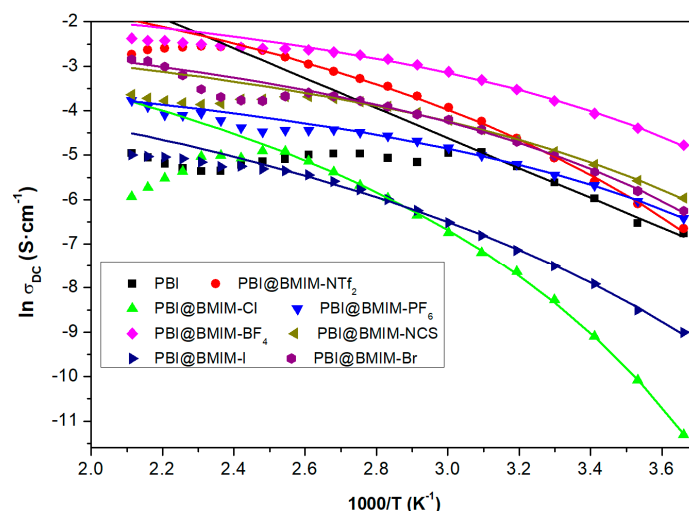


Figure 7. Variation of the $\ln \sigma_{dc}$ as a function of the reciprocal of the temperature for phosphoric acid doped PBI composite membranes containing 5 wt.% of 1-butyl-3-methylimidazolium (BMIM)-X (X: $[\text{NTf}_2]^-$, $[\text{Cl}]^-$, $[\text{BF}_4]^-$, $[\text{I}]^-$, $[\text{PF}_6]^-$, $[\text{NCS}]^-$ and $[\text{Br}]^-$). For comparison, the conductivity dependence with temperature for PBI pristine membrane doped with phosphoric acid is also given.

There are many examples of PBI composite membranes with values of proton conductivity and its corresponding activation energy. As an example, Wang and et al. [74] prepared an insoluble sulfonated polyphosphazene (SPOP) with 117% degree of sulfonation; the SPOP was used as the proton conductor in the PBI as HT-PEM, and the polyfunctional triglycidyl isocyanurate (TGIC) was used as a covalent cross-linking agent to inhibit swelling at low degree of cross linking of the PBI-TGIC/SPOP composite membranes obtained. The proton conduction activation energy was calculated at a specific set of RH and is summarized in Table 1. The conductivity of PBI-TGIC(5%)/SPOP(50%) at 100% RH, 50% RH, and 0% RH is 0.143, 0.076, and 0.044 S/cm at 180 °C, respectively. The authors described that the proton conduction activation energy increased with the increasing degree of crosslinking. This inhibited the water absorption of the composite membrane and hindered the passage in the membrane of the proton conduction through the vehicle mechanism. On the other hand, the increase of the doping amount of SPOP reduced the proton activation energy, because it promoted water absorption of the membrane and improved the connectivity of the hydrophilic regions in the membrane. When the RH% was lowered, the efficiency of the vehicle mechanism for conducting protons was reduced, thereby causing a decrease in proton conductivity and an increase in proton conduction activation energy. At 0% RH, the proton conduction mechanism of the PBI-TGIC/SPOP composite membrane is the hopping mechanism.

Table 1. Proton conduction activation energy calculated by polybenzimidazole (PBI)-triglycidyl isocyanurate (TGIC)/sulfonated polyphosphazene (SPOP) composite membranes.

Polymer	$E_{a(\text{RH } 100\%)} \text{ kJ/mol}$	$E_{a(\text{RH } 50\%)} \text{ kJ/mol}$	$E_{a(\text{RH } 0\%)} \text{ kJ/mol}$
PBI-TGIC(5%)/SPOP(50%)	12.7	19.5	24.3
PBI-TGIC(10%)/SPOP(50%)	14.1	20.8	25.2
PBI-TGIC(5%)/SPOP(40%)	16.2	22.1	26.7
PBI-TGIC(10%)/SPOP(40%)	18.6	23.5	27.1

Recently, Rajabi et al. prepared composite membranes by introducing melamine-based dendrimer amines (MDA) with mesoporous silica (SBA-15), and 1,3-di(3-methylimidazolium) propane dibromide dicationic ionic liquid ($\text{pr}(\text{mim})_2\text{Br}_2$) (DIL), the membranes were doped with PA and were used to improve the proton conductivity [75]. The APBI-DIL_{4.5}-MDA_{1.5} composite membranes exhibit a proton conductivity of 0.22 S/cm at 180 °C under dry conditions. With the increasing temperature,

the interaction between polymer chains decreases, leading to more mobility of proton carriers. The high mobility of protons and their access to the active sites can also have a positive effect on the E_a required for proton conduction through the Grotthuss and vehicular mechanisms in the membranes. According to the results displayed in Table 2, APBI-DIL_{4.5}-MDA_{1.5} composite membranes require a lower E_a to conduct the proton compared with the other membranes.

Table 2. Proton conduction activation energy calculated by APBI-dicationic ionic liquid (pr(mim)₂Br₂) (DIL)/mesoporous silica (MDA) composite membranes. PA, phosphoric acid.

Polymer	PA/PBI _{25 °C}	σ (S/cm)	E_a (kJ/mol)
APBI	7	0.051	21.20
APBI-DIL ₄	10.99	0.142	13.56
APBI-DIL _{4.5} -MDA _{0.5}	13.67	0.182	—
APBI-DIL _{4.5} -MDA _{1.5}	15.32	0.224	8.87
APBI-DIL _{4.5} -MDA _{2.0}	15.09	0.221	—

Compañ's working group [64] presents a systematic study of the physico-chemical properties and proton conductivity of PBI membranes doped with PA and other acids such as phytic acid and phosphotungstic acid (HPW). To further study the proton conduction mechanism of the membranes, the Arrhenius plots of the membranes and their proton conduction activation energy values (E_a) were analyzed; the results are presented in Table 3. Proton conductivity increases for all membranes from 20 to 180 °C, following typical Arrhenius behavior. The obtained values followed the trend: E_a (PBI-PA 14 M) < (PBI-PA 1 M) \approx (PBI-phytic) < (PBI-PA 0.1 M) < (PBI-HPW). These results indicate that proton mobilities increased with the amount of PA, and then PA formed channels in the organic phase of porous PBI. Similar activation energies were obtained for PBI-PA 1 M, PBI-PA 0.1 M, and PBI-phytic acid membranes, but PBI-PA 14 M displayed a lower value as the PA concentration was much higher and, therefore, the proton transport was more favored. According to these results, the Grotthuss mechanism dominates the proton transport in acid doped PBI membranes.

Table 3. Proton conduction activation energy calculated by PBI doped with different acids. HPW, phosphotungstic acid.

Polymer	σ_{DC} 140 °C (S/cm)	E_a (kJ/mol)
PBI	2.5×10^{-12}	53 ± 2
PBI-PA 1M	2.5×10^{-3}	25 ± 3
PBI-PA 14 M	5.3×10^{-2}	11.6 ± 0.7
PBI-phytic acid	2.6×10^{-4}	25 ± 2
PBI-HPW	1.9×10^{-11}	31 ± 3

In a recent publication of the group of Compañ, SiO₂ nanofiber mats were used as fillers in the preparation of composite PBI membranes for high temperature PEMFC applications [76]. In this work, SiO₂ nanofibers were fabricated through an electrospinning process and later functionalized using silane chemistry to introduce different polar groups, namely, -OH (neutral), -SO₃H (acidic), and -NH₂ (basic). The modified nanofiber mats were embedded in PBI to fabricate mixed matrix membranes. Proton conduction measurements show that PBI composite membranes containing nanofiber mats with basic groups showed higher proton conductivities. The E_a values of the composite membranes under wet conditions were lower than that for the pure PBI membrane, which is associated with an enhanced proton mobility, as the nanofiber acts as a carrier-bridge for protons and, consequently, the process demands less energy. On the one hand, the Grotthuss mechanism explains the conductivity by means of the interaction of protons through the jump between a hydrogen bond network of N-H groups, both from the PBI and from the functionalized groups of the nanofiber mats. On the other hand, protons can move via the vehicle mechanism through the hydroxyl, amine, or sulfonic groups

from the different nanofiber functionalization and imidazole groups present in the PBI, which may interact with water molecules, promoting the proton conductivity. Additionally, activation energies under dry conditions improve proton conduction, which is mainly owing to a vehicular mechanism, as inferred from the calculated activation energies, with values higher than 55 kJ/mol (see Table 4).

Table 4. Activation energies for the PBI composite membranes in wet and dry conditions for the temperature interval 20–90 °C.

Polymer	$E_{a(\text{wet})}$ kJ/mol	$E_{a(\text{dry})}$ kJ/mol
PBI	55.6 ± 0.8	75 ± 3
PBI-SiNF	12.7 ± 0.4	72 ± 3
PBI-SiNF-NH ₂	10.7 ± 0.3	56 ± 2
PBI-SiNF-SO ₃ H	25 ± 1.5	123 ± 10

In 2018, our research group described the preparation and characterization of composite PBI membranes containing zeolitic imidazolate framework (ZIF-8) and (ZIF-67) [77]. The calculated E_a associated with the proton transport in the PBI–ZIF-8 and PBI–ZIF-67 and PBI–ZIF–mix are shown in Table 5. Considering that the E_a for the PBI-ZIF membranes is lower than that for pure PBI membrane, it is suggested that the ZIFs clearly favor the conductivity of the membrane at moderate and high temperatures.

Table 5. Activation energies for the PBI composite membranes along the temperature interval 20–90 °C. ZIF, zeolitic imidazolate framework.

Polymer	E_a kJ/mol
PBI	36 ± 2
PBI–ZIF-8	33 ± 2
PBI–ZIF-67	30 ± 2
PBI–ZIF–mix	19 ± 1.4

According to the calculated activation energies, the proton conductivity could be rationalized by means of the Grotthuss mechanism by proton hopping through a network of hydrogen bonds along the polymeric matrix involving polybenzimidazole polymeric chains, phosphoric acid networks, and imidazolate rings from the ZIF (Figure 8).

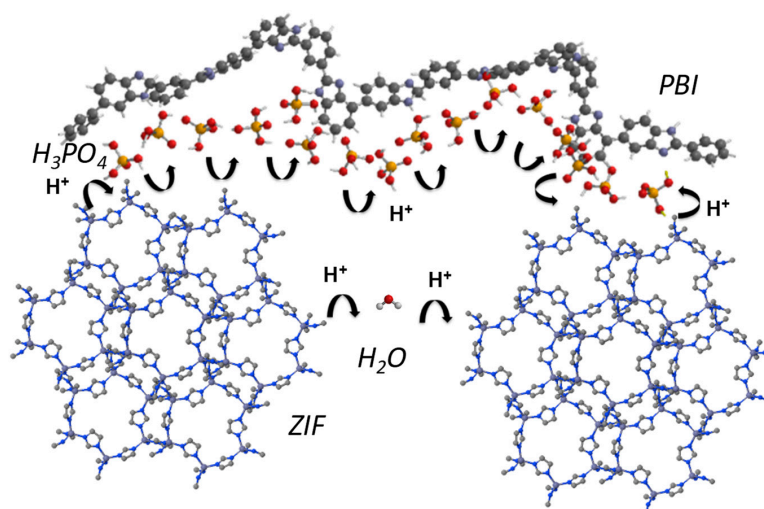


Figure 8. Schematic illustration of the possible mechanism for proton transfer in zeolitic imidazolate framework (ZIF)-containing PBI composite membranes. C, N, O, and P atoms are represented as grey, blue, red, and orange, respectively. H atoms are omitted from the ZIF structure for clarity [77].

Abouzari-Loft and co-workers used the 2,6-pyridine functionalized polybenzimidazole (Py-PBI) as substrate for hosting PA moiety. Phosphonated graphene oxide (PGO) was added to Py-PBI substrate at different levels prior to acid doping [78]. They found that the conductivity is more stable in the Py-PBI-PGO membranes. The proton conductivity of the membranes showed a temperature dependence, that is, an Arrhenius-type of behavior in the whole range of temperatures. The activation energy for the Py-PBI based membrane was lower for the composite membranes with 1.0% and 1.5% PGO contents, as shown in Table 6. The authors proposed that such a reduction in the E_a for the PGO containing membranes may indicate the synergic effect of the phosphonated PGO filler in boosting the membrane proton conductivity. The presence of PGO with an exfoliated structure may have disrupted the crystalline structure of PyPBI, which results in more available and stronger sites for PA trapping and provided additional diffusion pathways for proton hopping across the membrane via the Grotthuss mechanism.

Table 6. Activation energies for the PyPBI-phosphonated graphene oxide (PGO) composite membranes doped PA.

Polymer	$E_{a(\text{dry})}$ kJ/mol
PyPBI	22.8
PyPBI-PGO _{1.0}	18.2
PyPBI-PGO _{1.5}	18.0

3. Influence of the PBI Structure and Synthetic Methods on Its Conductivity

As mentioned above, PBIs, owing to their excellent mechanical properties and high chemical resistance, are considered as the most important polymers for the fabrication of membranes to work at high temperatures in the construction of stacks for HT-PEMFCs. The PBI membranes are generally prepared by casting from polymer solutions and then doped with acid, although a direct method for casting the PBI together with acid has also been developed [79,80].

The structure of PBI has an important effect on many of its properties such as solubility, stability, and proton conductivity. PBIs have a poor solubility owing to their rigid structure. Another important factor affecting the solubility is the molecular weight of the polymer. In this regard, PBIs with molecular weights ranging from 23 to 37 kDa have relatively good solubility, but polymers with lower molecular weights are not strong enough to ensure fuel cell requirements. However, polymers with higher molecular weights are found to be poorly soluble in polar organic solvents. Therefore, many approaches have been used to improve both the strength and solubility of PBI [81,82].

One strategy to strengthen and make PBI more soluble consists of introducing a flexible group in the backbone, such as ether linkages, that facilitates the chain mobility, and consequently solubility, and simultaneously enhances the molecular weight of the PBI and its strength. PBIs containing ether units have been synthesized and applied as polymeric electrolytes for HT-PEMFCs. Furthermore, the introduction of ether units in the PBI has been reported an effective method of increasing the proton conductivity of the membranes. So, the synthesis of poly [2,2'-(*p*-oxydiphenylene)-5,5'-benzimidazole] (OPBI) obtained by polycondensation of 3,3'-diaminobenzidine (DAB) and 4,4'-oxybisbenzoic acid (OBBA) was reported (Figure 9), and the membrane prepared from this polymer, after PA doping, which showed values of proton conductivity up to 0.083 S/cm at 150 °C under anhydrous conditions [83]. The fabricated PBI/PA MEA was tested for 100 h without any degradation in voltage noticed, reaching maximum power and current densities of 1.17 W/cm² and 6.0 A/cm², respectively (Figure 10).

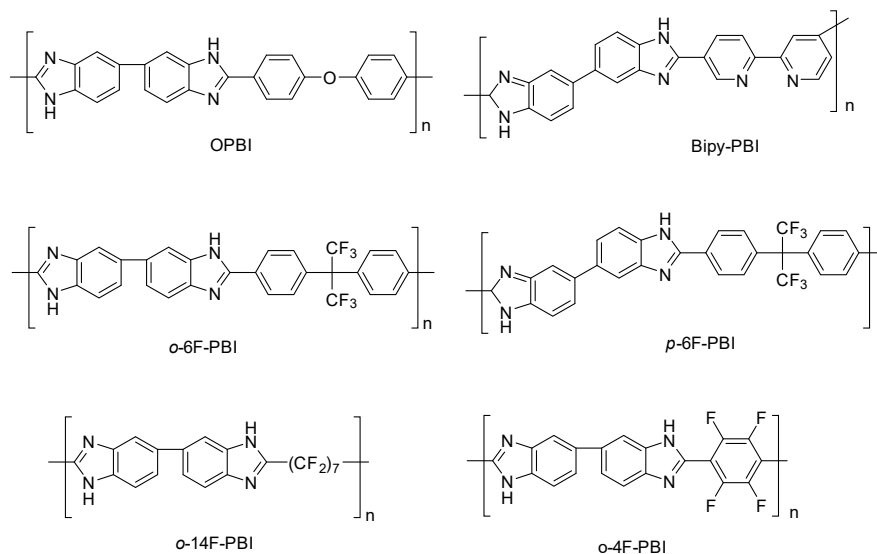


Figure 9. Different structures of PBIs.

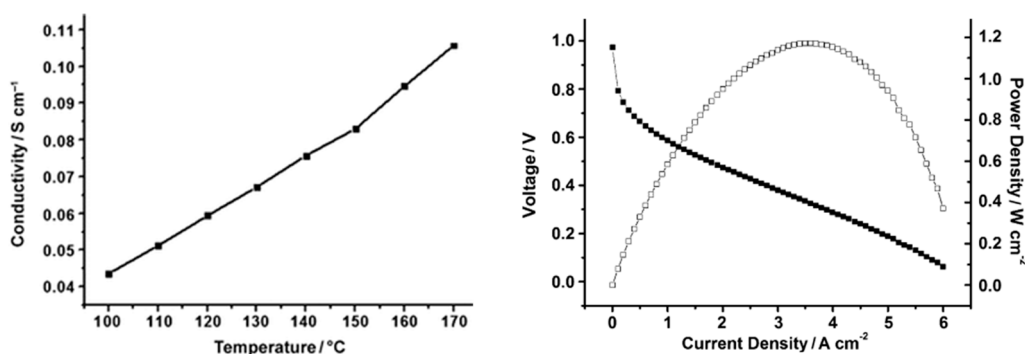


Figure 10. Variation of conductivity of PA doped OPBI with temperature (left) and fuel cell performance (■: voltage, □: power density) of the OPBI membrane (right). Reproduced from [83] with permission of John Wiley and Sons.

In 2019, Berber and Nakashima described the synthesis of bipyridine-based polybenzimidazole (Bipy-PBI) of various molecular weights and it was concluded that the molecular weight significantly affected thermal stability, mechanical properties, proton conductivity, and FC performance of the membranes [84]. The conductivity of the 141 kDa Bipy-PBI membrane reached 0.037 S/cm at 120 °C and anhydrous conditions, with a maximum power density of 0.78 W/cm² and a current density at 0.5 V of 1.6 A/cm².

An alternative synthesis of OPBI by microwave irradiation was also reported by Kang and coworkers [85]. The proton conductivity of the H₂SO₄-doped membranes prepared from this PBI showed values up to 0.190 S/cm at 160 °C and anhydrous conditions. The synthesis of porous and asymmetric OPBI without the use of any porogenic additive was also developed by Ou and coworkers; the conductivity of 0.072 S/cm at 180 °C for such OPBI membrane was reported and a peak power density of 0.4 W/cm² at 160 °C under anhydrous conditions was reached in the fuel cell test [86].

The incorporation of hexafluoroisopropylidene groups in the polymeric structure has been efficiently used to improve the proton conductivity of polyimides and polyamides [87]. Consequently, such an approach was tried on PBI membranes. In this regard, Qian and Benicewicz prepared a hexafluoroisopropylidene-containing *o*-polybenzimidazole (*o*-6F-PBI) membrane with a proton conductivity of 0.09 S/cm at 180 °C after phosphoric acid doping and a fuel cell performance with a maximum power density of 0.58 W/cm² 0.2 A/cm² was described [88]. A year later, another hexafluoroisopropylidene-containing PBI (*m*-6F-PBI) was synthesized and the PA-doped membrane

exhibited a proton conductivity of 0.02 S/cm at 180 °C, and a peak power density of 0.574 W/cm² at 0.2 A/cm² at 180 °C. The synthesis of other fluorinated PBIs, such as poly(2,2'-(tetrafluoro-*p*-phenylene)-5,5'-bibenzimidazole) (*o*-4F-PBI) and poly(2,2'-tetradecafluoroheptylene-5,5'-bibenzimidazole) (*o*-14F-PBI), has been described, and their PA-doped membranes reached conductivity values up to 0.03 S/cm at 150 °C. The crosslinked *m*-6F-PBI membranes using epoxide cross-linkers were prepared. The membranes showed high acid doping level, enhanced mechanical strength, and oxidation stability in comparison with the pure *m*-6F-PBI. Additionally, the proton conductivity in these cross-linked PA-doped membranes reached values up to 0.060 S/cm at 160 °C and a current density of 0.634 A/cm² at 0.51 V [89].

Chemical modification of PBI by means of click chemistry reactions [90] and by the alternative and environmental friendly metal-free click chemistry reactions [91], such as the strain-promoted azide-alkyne cycloaddition (SPAAC) [92], the thiol-ene [93,94] and thiol-yne coupling [95,96], the inverse electron-demand Diels-Alder (IEDDA) reaction [97], the strain-promoted alkyne-nitrone cycloaddition (SPAN) [98,99], and the strain-promoted oxidation-controlled cyclooctyne-1,2-quinone cycloaddition (SPOCQ) [100–102], can afford an interesting variety of PBI structures with potential applications in PEM for fuel cell applications. The main advantages of these reactions include their fast reaction kinetics, versatility and regiospecificity, high product yields, and easy purification of the products. In this regard, these methodologies have been efficiently used along the past decade in the preparation of polymers [103], but their application in fuel cells remains almost unexplored.

4. Copolymers

Another commonly used alternative to fabricate PBI-based polymers with desirable properties (high proton conductivity in combination with high chemical and thermal stability and adequate mechanical properties) is based on the preparation of PBI copolymers [104]. On these lines, copolymerization has attracted researchers' interest in the last decade as it allows a fine tuning of the polymer properties by simply selecting the monomer concentration/monomer ratio in the copolymer (Figure 11) [105].

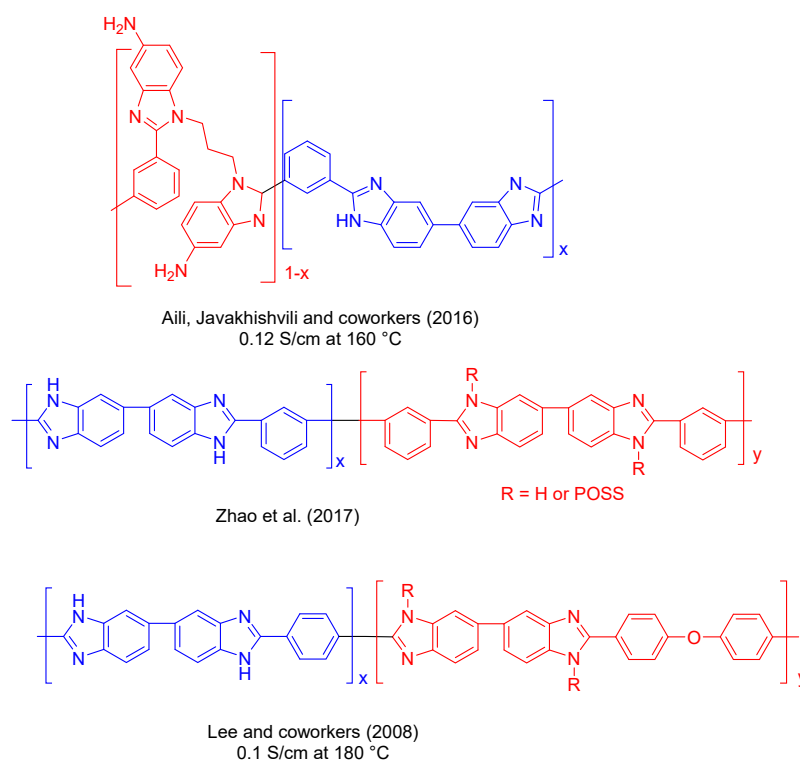


Figure 11. Different copolymers of PBI. POSS, polyhedral oligosilsesquioxane.

Aili, Javakhishvili, and coworkers have synthesized an amino-functional benzimidazole copolymer by condensation of isophthalic acid, 3,3'-diaminobenzidine, and new a hexamine, *N,N'*-bis(2,4-diaminophenyl)-1,3-diaminopropane (Figure 11). Blend membranes prepared with conventional PBI showed proton conductivities up to 0.12 S/cm at 160 °C after phosphoric acid doping [106], which was in accordance with the observed high acid uptakes. Zhao et al. synthesized a series of grafted polybenzimidazole copolymers containing polyhedral oligosilsesquioxane (POSS) pendant moieties, which are a family of well-defined cage-like molecules (Figure 11) [107]. These copolymers exhibited improved mechanical properties over pristine PBI, with a Young's modulus of ~5 GPa and tensile strength of 85 MPa; whereas for pristine PBI, the values were of 1.36 GPa and 71 MPa, respectively. Another copolymerization approach described by McGrath and coworkers was based on multiblock copolymers containing different block lengths. These copolymers were prepared by coupling carboxyl functional aromatic poly (arylene ethers) with ortho diamino functional PBI oligomers in different poly(arylene ether sulfone) and PBI ratios [108]. Using a similar approach, Lee and coworkers described the synthesis of poly (aryl ether benzimidazole) copolymers containing different contents of aryl ether linkages by condensation of 4,4-dicarboxydiphenyl ether (DCPE) and terephthalic acid (TA) by varying the DCPE/TA ratio (Figure 11). The authors concluded that the optimal content of aryl ether linkages was 10–30 mol %. With this approach and after PA doping, membranes displayed a proton conductivity of 0.1 S/cm at 180 °C [109].

The group of Benicewicz has deeply explored the synthesis of new compositions to improve the chemical, thermal, and mechanical stability, as well as proton conductivity, of PBI-based membranes. In 2005, a series of *meta/para*-PBI random copolymer membranes were fabricated by Benicewicz and coworkers via a phosphoric acid sol–gel process. These copolymers exhibited a maximum proton conductivity of 0.26 S/cm at 180 °C with a high acid doping level, which was efficiently retained in the membrane [110]. Fuel cell tests displayed a current density of 0.2 A/cm² and a voltage around 0.65 V at temperatures above 150 °C without any feed gas humidification, and were stable for more than 1000 h. In 2011, Mader and Benicewicz reported the preparation of PBI containing sulphonic acid groups by copolymerization of *p*-PBI with polyphosphoric acid (PPA), which displayed excellent proton conductivities with values close to 0.3 S/cm at 180 °C [111]. The authors used different segmented block copolymers containing *p*-PBI and sulphonated PBI (*s*-PBI) in different ratios for the preparation of membranes, which displayed fuel cell performances at 160 °C with voltages around 0.74 V at 0.2 A/cm². The highest conductivity was found for the 25:75 *s*-PBI/*p*-PBI membrane (0.376 S/cm). The same group has also described the preparation of polyphenylquinoxaline-based PBI copolymers via the polyphosphoric acid (PPA) process with proton conductivities up to 0.26 S/cm [112]. Using the PPA process, a series of pyridine-containing *m*-PBI copolymers were used for the preparation of membranes with enhanced mechanical properties, which displayed a proton conductivity of 0.16 S/cm at 160 °C [113]. Fuel cell performances of these membranes were similar to those of *para*-PBI and long-term stability showed these copolymers maintained a consistent fuel cell voltage of 0.6 V at 0.2 A/cm² for over 2300 h. In a later study, the long-term stability was extended to more than 8000 h [114]. A series of PBI-based block copolymers consisting of phosphophilic PBI and phosphophobic non-PBI segments were synthesized via coupling of ortho-diamino terminated *meta*-PBI telechelic macromonomers and carboxylic acid end-capped poly (arylene ether) telechelic macromonomers (Figure 12). The block copolymer PBI-fluorinated poly (arylene ether) displayed a conductivity up to 0.11 S/cm after doping with concentrated PA, but having low mechanical properties [115]. The fuel cell performance showed a 20 μV/h degradation rate when operating at 0.2 A/cm² over 2000 h with an initial 0.58 V at 0.2 A/cm².

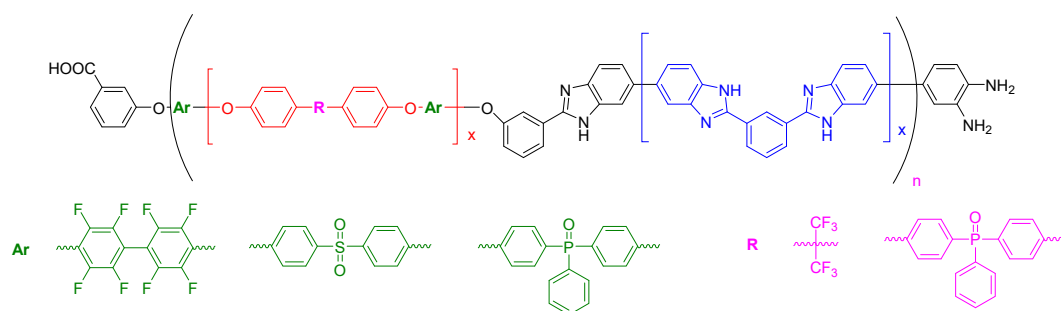


Figure 12. PBI-based block copolymers of phosphophilic PBI and phosphophobic non-PBI segments [115].

Maity and Jana reported the synthesis of a series of *meta*-PBI-block-*para*-PBI segmented block copolymers with different block lengths by the condensation reaction of diamine-terminated *meta*-PBI and acid-terminated *para*-PBI oligomers [116]. The maximum proton conductivity for this block copolymer was 0.11 S/cm at 160 °C, displaying a block structural influence on the proton conductivity. Pan and coworkers synthesized a series of sulfonated polybenzimidazole multiblock copolymers containing pyridine rings via the condensation polymerization of a dicarboxyl monomer containing pyridine, 3,3',4,4'-tetraaminobiphenyl, and 4-aminobenzoic acid in polyphosphoric acid. Next, membranes were prepared via the generally used solution casting method and subsequently doped with phosphoric acid [117]. The prepared membranes displayed an improved thermal and oxidative stability, reaching proton conductivities up to 0.23 S/cm at 180 °C.

Co-polymers of ABPBIs containing phenoxy in the main chain were synthesized by Wang and coworkers via the solution casting method. The copolymers were synthesized by copolymerization of 3,4-diaminobenzoic acid (DABA) and 4-(3,4-diaminophenoxy)benzoic acid (DPBA) under microwave irradiation. The polymeric membranes displayed an improved stability in organic solvents with proton conductivities up to 0.05 S/cm at 160 °C for the PA-doped membranes (Figure 13); however, a low tensile strength of ~2 MPa was reached after acid doping [118]. Kim et al. prepared cross-linked copolymer membranes of polybenzimidazole and polybenzoxazine [119]. The copolymerized membranes showed a maximum proton conductivity of 0.12 S/cm at 150 °C under anhydrous conditions. Fuel cell tests showed operating voltages of 0.71 V at 0.2 A/cm², with an excellent long-term durability up to 2000 operating cycles.

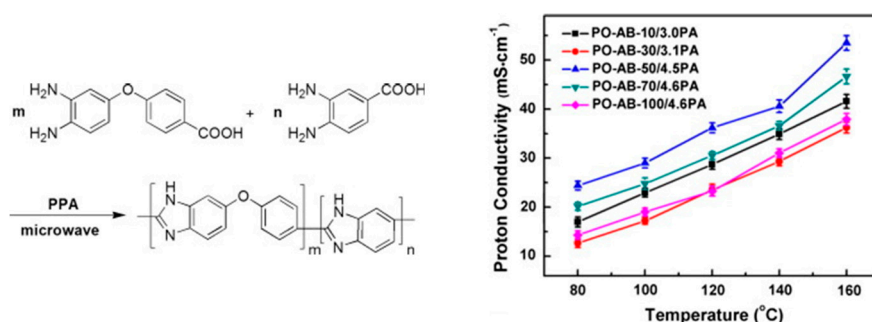


Figure 13. Synthetic route of phenoxy-containing ABPBI (left) and (right) proton conductivity of PO-AB-x membranes as a function of temperature (PO-AB-x, x refers to the molar feed percent of 4-(3,4-diaminophenoxy)benzoic acid (DPBA) in total monomers). Reproduced from [118] with permission of Elsevier.

5. Composite Membranes

Development of the composite PBI membranes, i.e., appropriate combination of inorganic-organic hybrid materials and polymer matrix, allowed significant improvement in the proton conductivity [120].

These composite materials are very attractive since they take advantage of the properties of inorganic and polymeric materials. Moreover, introduction of various inorganic or organometallic fillers into the same polymer matrix results in formation of novel materials. Different fillers were proposed for improving the mechanical integrity of PBI composite membranes. As a first generation, such fillers as silica (SiO₂) [121], titanium (TiO₂) [122], zirconia (ZrO₂) [123], and carbon materials [124] were reported to improve the dimensional stability, mechanical properties and gas permeability of PBI composite membranes. Recently, a second generation of acid functionalized fillers have received growing attention due to the mutual contribution to the proton transport. In this regards, various carbon-based substrates including graphene oxide (GO) [125,126] and carbon nanotubes (CNTs) [127], ionic liquids (ILs) [128], metal organic frameworks (MOFs) [77], nanofibers [129], among others were reported.

The properties of PBI composite membranes classified by the type of filler are outlined as follows.

5.1. PBI/Inorganic Composite Membranes

In order to address limitation issues in PA doped PBI membranes, such as low mechanical properties caused by high doping level and acid leaching from the membrane in extreme temperatures, the most widely used approach is the incorporation of an inorganic filler. Introducing various inorganic fillers greatly contributes to the improvement of the membrane behavior and its intrinsic ability to conduct protons. It was found that the addition of inorganic material to PBI to obtain composite or nanocomposite membranes allowed to improve the proton conductivity, water/PA uptake and retention, durability, high mechanical, thermal, and chemical stability at high temperatures, as well as overall fuel cell performance [130,131].

5.1.1. Metallic Oxides

Metallic oxide fillers such as SiO₂, TiO₂, and ZrO₂ were introduced into PBI matrices and some improvements in terms of dimensional stability, mechanical properties, and gas permeability of such formed composite membranes were observed. Over the past decade, a significant increase in the use of fillers based on metallic oxide compounds has been observed for fuel cell applications, as can be seen in Figure 14. As shown in Table 7, proton conductivity values close to 0.12 S/cm can be reached using metallic oxides as inorganic fillers in composite PBI membranes.

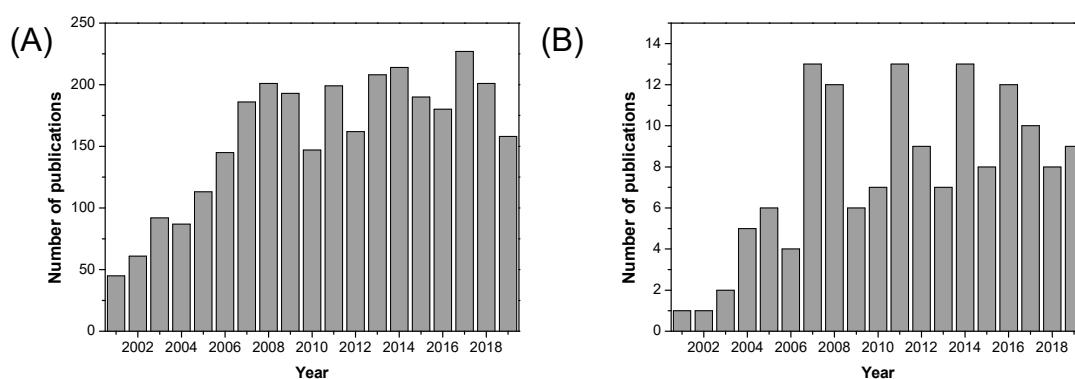


Figure 14. Number of publications in the period of 2001–2019 indexed in the Web of Science: (A) keywords: metallic oxide AND fuel cell; and (B) keywords: metallic oxide AND fuel cell AND proton exchange membrane. Source: www.webofknowledge.com.

Pu and coworkers [132] prepared PBI/SiO₂ composites with up to 15% SiO₂ content; the membranes were thermally stable up to 600 °C and generally exhibited better mechanical properties than the PBI membranes of the same structure, but without the filler. A decrease in the tensile strength was observed only at higher SiO₂ content. The membranes had proton conductivity of 3.9×10^{-3} S/cm at 180 °C. Later, Devrim and collaborators [133] prepared PBI/SiO₂ membranes that were tested in single cell HT-PEMFC; they exhibited higher proton conductivity of 0.103 S/cm at 180 °C. For comparison, the conductivity of

the same PBI membrane without filler was 0.094 S/cm. Many efforts have been devoted to improving the compatibility and membrane properties, studying combinations of various metals or modified metal oxide structures as fillers. For example, high conductivity of 0.31 S/cm was obtained for composite membranes filled with mixed Al-Si. The filler was readily produced by the sol-gel method [134]. The proton conductivity and MEA performance of PBI/Al-Si composite were improved with the increasing Al-Si concentration, but the mechanical properties were not desirable, as they got worse. Lysova and coworkers prepared a polybenzimidazole based on 3,3',4,4'-tetraaminodiphenyloxide and 3,3'-bis(p-carboxyphenyl)phtalide (PBI-O-PhT) and formed composite membranes using SiO₂ or ZrO₂ added by two different methods: (1) addition of preliminarily synthesized particles in situ during the polymer synthesis and (2) addition during the casting [135]. It was shown that the modification by zirconia with the in situ method improved the ionic conductivity better than the modification by silica. In the case of the casting method, better results were obtained for silica modification. Zhang and coworkers prepared a membrane using an OPBI polymer and zirconium phosphate (Zr(HPO₄)₂·nH₂O, ZrP) [136]. The PBI/ZrP exhibited excellent mechanical strength with 10 wt.% ZrP and showed the highest proton conductivity of 0.192 S/cm at 160 °C under anhydrous condition. Lobato and coworkers prepared membranes PBI by casting in the presence of 2 wt.% TiO₂, and the fuel cell with this composite showed better performance compared with the fuel cell with the standard PBI membranes, achieving 1000 mW/cm² at 175 °C [137]. The study of PBI composites using mixed Fe₂TiO₅ oxides was also performed [138]. According to the Lewis acid-base theory, the main cations Ti⁴⁺ and Fe³⁺ are classified as hard acids [139]. This means that they may easily react with OH of water. Additionally, it was suggested that, when Fe³⁺ cations were placed near Ti⁴⁺ cations, as occurred in the Fe₂TiO₅ structure, their acidity was increased. Therefore, Fe₂TiO₅ single-phase nanoparticles were more hydrophilic than both TiO₂ and Fe₂O₃ nanoparticles separately [140]. The PBI/Fe₂TiO₅ membranes showed a higher acid uptake and proton conductivity compared with the pure PBI membranes. The proton conductivity of 0.078 S/cm at 180 °C was observed for the PBI/Fe₂TiO₅ containing 4 wt.% of nanoparticles.

Table 7. Composite membranes of polybenzimidazole derivates with inorganic materials.

Polymer	Filler	wt.%	σ_{DC} (S/cm)	T (°C)	Doped	Ref
PBI	—	—	10 ⁻¹²	160	—	[64]
PBI	SiO ₂	15	0.004	180	—	[132]
PBI	SiO ₂	5	0.103	180	—	[121]
PBI	Al-Si	—	0.310	—	—	[134]
PBI-O-PhT	ZrO ₂	-	0.162	180	D	[135]
OPBI	α -ZrP	10	0.192	160	—	[136]
PBI	TiO ₂	2	0.081	175	—	[137]
PBI	Fe ₂ TiO ₅	4	0.078	180	D	[138]
PBI	SiWA-SiO ₂	50	0.001	160	—	[141]
PBI	SiWA-SiO ₂	50	0.002	160	D	[141]
PBI	ZrP	15	0.096	200	D	[142]
PBI	BPO ₄	25	0.027	180	D	[142]
PBI	CsPOMo	30	0.120	160	D	[143]
PBI	CsPOW	30	0.100	160	D	[143]
PBI	CsSiOW	30	0.057	160	D	[143]
PBI	CsSiMo	30	0.051	160	D	[143]
PBI	BaZrO ₃	4	0.125	180	D	[144]

The composite membranes prepared from silicotungstic acid supported on silica (SiWA-SiO₂/PBI) were studied by Staiti [141]. The silica was necessary to entrap the acid, averting its dissolution in water, and to improve the proton conduction. The best result was obtained for the membrane with 50 wt.% of inorganic material; it was mechanically stable and gave a proton conductivity of 1.2×10^{-3} S/cm at 160 °C and 100% RH, while the membranes prepared with pure silicotungstic acid had a conductivity of 2.23×10^{-3} S/cm under the same conditions.

PA-doped PBIs containing inorganic proton conductors such as zirconium phosphate (ZrP) ($\text{Zr}(\text{HPO}_4)_2 \cdot n\text{H}_2\text{O}$), phosphotungstic acid (PWA) ($\text{H}_3\text{PW}_{12}\text{O}_{40} \cdot n\text{H}_2\text{O}$), and silicotungstic acid (SiWA) ($\text{H}_4\text{SiW}_{12}\text{O}_{40} \cdot n\text{H}_2\text{O}$), or boron (BPO_4), were investigated by Di et al. [142]. It was concluded that the conductivity of these composite membranes depended on the acid doping level, RH, and temperature, similar to simple PA-doped PBIs. The conductivity was found to be insignificantly higher for the inorganic composite membranes.

Xu et al. [143] presented different PBI-based inorganic–organic composite membranes from Cs substituted heteropolyacids (CsHPAs) with the intention to build MEA for application at intermediate and high temperatures. The CsHPA/PBI membranes loaded with H_3PO_4 had much higher conductivity than that of PA-doped PBI. It was observed that conductivity increased with an increase of the filler in the composite. The membrane of 30% CsPOMo/PBI with a doping level of 4.5 exhibited conductivity as high as 0.12 S/cm at 150 °C and anhydrous conditions, and additionally demonstrated excellent mechanical behavior with a strength of 40 MPa. The performance of CsPOMo/PBI/ H_3PO_4 membranes in a H_2/O_2 single fuel cell was also very good, holding a power density of around 0.6 W cm^{-2} with oxygen at atmospheric pressure.

Hooshyari et al. [144] studied the behavior of PBI-BaZrO₃ (PBZ) nanocomposite membranes for HT-PEMFC; their results showed that the water uptake, acid doping level, and proton conductivity of the PBZ were higher than that of the virgin PBI membrane owing to the presence of BaZrO₃ perovskite nanoparticles (Figure 15). The proton conductivity observed for these composites containing 4 wt.% of the nanofillers was around 0.125 S/cm at 180 °C, and the performance in a mono fuel cell produced a power density at 0.5 V and 180 °C of 0.56 W/cm^2 , below a 5% RH with a current density of 1.12 A/cm^2 . These results indicate that such membranes are excellent candidates for HT-PEMFC.

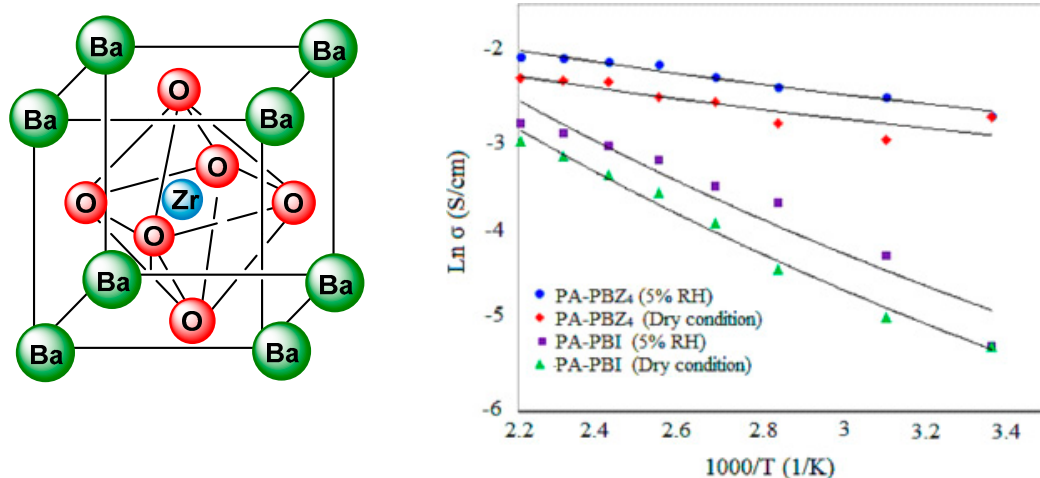


Figure 15. Structure of BaZrO₃ nanoparticles and Arrhenius plot of proton conductivity for PA-PBI and PA-PBZ₄ membranes, where Z₄ means the content of perovskite is 4 wt.%. Reproduced from [144] with permission of Elsevier.

Akbar et al. studied the composite membranes using perovskite-type SrCeO₃ nanoparticles for improving their properties at high temperatures for the application in HT-PEMFC [145]. The PA-doped PBI/SrCeO₃ membranes showed higher acid uptake (190%), excellent proton conductivity (0.105 S/cm at 180 °C), and better thermal stability at 8 wt.% of SrCeO₃ (PSC₈) content in comparison with the pure PBI membrane. The performance of the PSC₈ nanocomposite membrane showed a 0.44 W/cm^2 power density and 0.88 A/cm^2 current density at 0.5 V and 180 °C. The results obtained in these studies clearly demonstrated the enhanced potential of the PSC₈ as PEM for high temperature proton exchange membrane fuel cells.

5.1.2. Metallocarboranes

Our group, in collaboration with the group of F. Teixidor, has also studied a family of inorganic fillers based on sandwich compounds of molecular formula $M[\text{Co}(\text{C}_2\text{B}_9\text{H}_{11})_2]$ ($M = \text{Li}^+, \text{Na}^+, \text{H}^+$), also named $M[\text{COSANE}]$ (Figure 16). These compounds are highly stable anionic materials with a very low charge density. In 2017, we investigated the temperature dependence of the proton conductivity of the cobalt salt $\text{H}[\text{COSANE}]$ under wet and dry conditions. We observed that conductivity was strongly dependent on the relative humidity and was higher in $\text{H}[\text{COSANE}]$ than in other metallocarboranes from the same family such as $\text{Na}[\text{COSANE}]$ or $\text{Li}[\text{COSANE}]$. In this regard, the observed conductivity of $\text{H}[\text{COSANE}]$ was similar to that of other PBI membranes containing carboxylic groups and inorganic fillers, reaching values up to 0.01 S/cm [146]. Recently, we have used these fillers in the preparation of composite proton exchange membranes based on PBI. In a cation study, using $\text{H}[\text{COSANE}]$, $\text{Li}[\text{COSANE}]$, and $\text{Na}[\text{COSANE}]$ fillers, the conductivity of the composite membranes followed the trend $\sigma(\text{PBI@H}[\text{COSANE}]) > \sigma(\text{PBI@Na}[\text{COSANE}]) > \sigma(\text{PBI@Li}[\text{COSANE}])$, reaching values close to 0.001 S/cm [147]. The electrochemical impedance spectroscopy results showed that conductivity increased with temperature and is higher for H^+ than for Li^+ and Na^+ for all temperatures under study. The temperature dependence of the conductivity of the composite was followed by a typical Arrhenius behavior with two different regions: (i) between 20 and $100 \text{ }^\circ\text{C}$ and (ii) between 100 and $150 \text{ }^\circ\text{C}$, whose activation energy values are given in Table 8. The pristine PBI membranes show that the conductivity strongly begins to fall down, which may be because of the hydration of the membrane when the temperature is higher than $100 \text{ }^\circ\text{C}$. However, for the PBI composite membrane, the authors observed a second behavior between 100 and $150 \text{ }^\circ\text{C}$, where the conductivity tends to increase with a different slope compared with the first interval up to $150 \text{ }^\circ\text{C}$. At temperatures above $150 \text{ }^\circ\text{C}$, in composite membranes, conductivities decreased when temperature increased. This is possible owing to the solvent evaporation temperature used in membranes' preparation. The evaporation temperature of solvent (DMAc) is about $160 \text{ }^\circ\text{C}$, which could explain why membrane conductivity was found to be reduced above this temperature value.

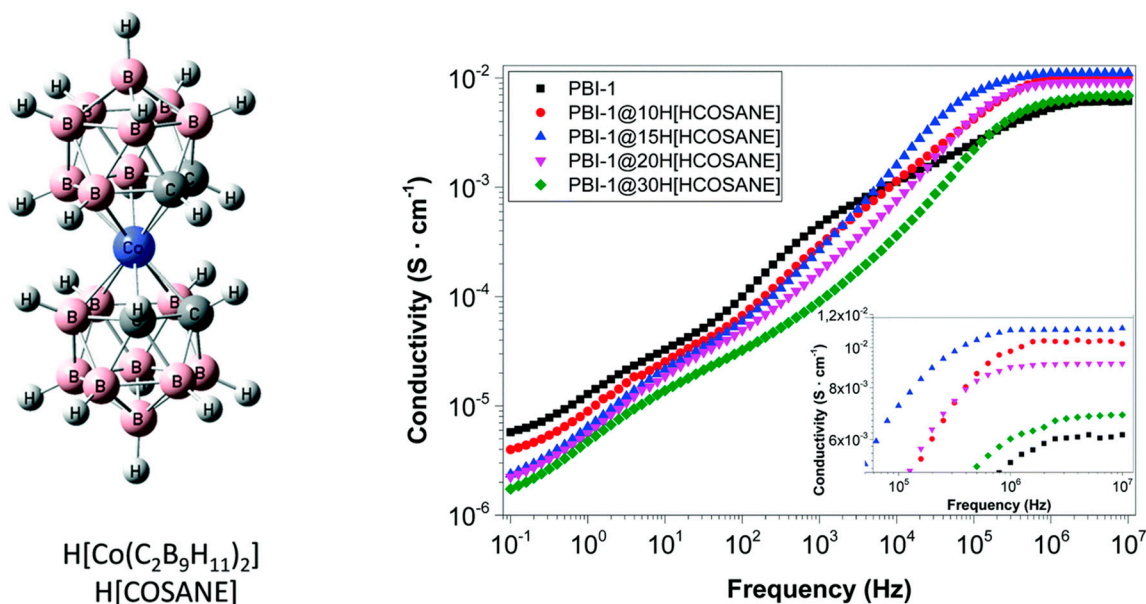


Figure 16. Ball and stick view of $\text{H}[\text{COSANE}]$ (left) and Bode diagram for composite membranes of PBI containing 15 wt.% of $\text{H}[\text{COSANE}]$ (right). Reproduced from [148] with permission of the Royal Society of Chemistry.

Table 8. Activation energy values for PBI, PBI@M[COSANE], and PBI@M[TPB] membranes.

Membrane	E_a (kJ/mol) $T \in [20\text{--}100\text{ }^\circ\text{C}]$	E_a (kJ/mol) $T \in [100\text{--}150\text{ }^\circ\text{C}]$
PBI@H[COSANE]	24.7 ± 0.7	5.6 ± 0.1
PBI@Li[COSANE]	19.1 ± 0.8	3.9 ± 0.4
PBI@Na[COSANE]	26.1 ± 1.2	5.2 ± 0.3
PBI@Li[TPB]	29.5 ± 0.9	6.1 ± 0.6
PBI@Na[TPB]	29.1 ± 1.6	7.3 ± 0.3
PBI	20.5 ± 2.3	—

In a recent study, the effect of the H[COSANE] concentration in three different polymeric matrices based on the PBI structure, PBI, OPBI, and *o*-6F-PBI have been investigated [148]. All prepared membranes displayed excellent proton conductivities higher than 0.03 S/cm above 140 °C, reaching a maximum when the amount of H[COSANE] was 15 wt.%.

5.2. Graphene Oxide, Carbon Nanotubes, and Others

Another type of filler that has been attracting attention for the last two decades is the family of graphene nanomaterials, mostly in the form of nanotubes or graphene oxide (GO). In particular, GO has received special interest because of the unique combination of its properties, as can be shown by the number of publications over the last decade (Figure 17). GO is formed from the oxidation of graphite and comprises 2D carbon sheets, but is decorated with oxygen-containing functionalities on the edges (hydroxyl, carbonyl, and carboxyl groups) and on the surface (hydroxyl and epoxide groups) [149,150].

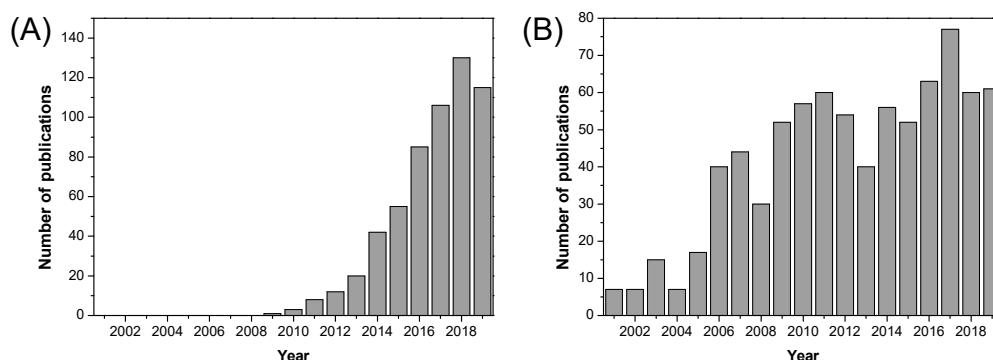


Figure 17. Number of publications in the period of 2001–2019 indexed in the Web of Science: (A) keywords: graphene oxide AND fuel cell AND proton exchange membrane; and (B) keywords: carbon nanotube AND fuel cell AND proton exchange membrane. Source: www.webofknowledge.com.

Thus, GO maintains all exceptional properties of graphene, but in contrast to graphene, GO is easily dispersible in water, organic solvents, or polymer matrices owing to the presence of the oxygen functionalities, whereas graphene has a strong tendency to agglomerate. The use of GO as a precursor is the most reliable and effective approach for preparing graphene-based polymer composites. GO typically preserves the layer structure of the graphite, but the layers are buckled and the interlayer spacing is much larger than the graphite [151]. GO is an electronic insulator with differential conductivity; however, when GO is added into a polymer matrix, the protons presented in the membrane interact with GO, and this promotes proton conductivity on the composite membrane [152]. Owing to its unique properties, GO has found tremendous applications in a diverse range of fields, such as gas barrier nanocomposites [153], water treatment [154], stimuli-responsive materials [155], energy storage as supercapacitors [156], lithium ion batteries [157], and stretchable electronics [158].

The presence of GO in the membrane provides the advantages of excellent mechanical properties, large specific surface area, and as high as 0.01 S/cm inherent proton conductivity. Therefore, the introduction of

GO into the PBI polymer matrix helps to improve the acid doping and proton conductivity, and prevent acid leaching. Besides, GO allows improving the performance and increasing the durability of HT-PEMFC. As shown in Table 9, proton conductivity values close to 0.17 S/cm can be reached using GO as a filler in PBI membranes.

Üregen and coworkers prepared and studied a PBI/GO nanocomposite with different weight percentage GO loading [38]. The maximum proton conductivity of 0.17 S/cm at 165 °C was observed for the membrane with 2 wt.% GO content. The membrane performance in the HT-PEMFC system showed that it was significantly improved in comparison with the pristine PBI membrane under dry conditions. In the last years, attempts to apply GO modified with sulfonated, phosphonated, and other groups have been made in order to improve proton conductivity, as well as dispersion and compatibility between the filler and polymeric matrix. Yang and coworkers prepared a PBI composite membrane with GO bearing triazole groups (TrGO) [159]. The presence of triazole functionality allowed improving the compatibility with the polymer. The PBI/TrGO membranes with 1.2 wt.% of TrGO were much more uniform and homogeneous than the PBI/GO membranes. The last ones were quite heterogeneous and demonstrated obvious phase-separation. The tensile strength of the PA doped composite membranes was 12.6 MPa, which was much higher than that of the PBI membrane with a similar acid doping level (ADL) of around 12. Moreover, the high proton conductivity of 0.135 S/cm at 180 °C was achieved in this membrane.

Cai and coworkers prepared sulfonated GO (SGO), using the ^{60}Co γ -ray radiation grafting method, which was then added into PBI via solution-casting [126]. The sulfonic acid groups in SGO were able to form stronger interactions with the $-\text{N} = \text{O}$ or $-\text{NH}$ groups of the benzimidazole ring than the oxygen-containing groups of the non-modified GO, and thus SGO was well dispersed in the polymer even with the SGO content of 1 wt.% (PBI/SGO-1%). Additionally, the composite exhibited much better mechanical properties, with a tensile strength of 133.1 MPa, an elongation at break of 36.4%, and a tensile modulus of 2134 MPa. These values increased in 32.0%, 220%, and 33% compared with those for pure PBI membrane, respectively. However, when SGO content was $>1\%$, low dispersion in the polymer matrix led to a reduction in the mechanical properties of the membranes. The proton conductivity of PBI/SGO-1%/PA was 0.023 S/cm at 170 °C under dry conditions (Figure 18). Then, composites of 2,6-pyridine functionalized PBI with highly dispersible phosphoric acid functionalized GO (PGO) were proposed as candidates for durable performance at elevated temperature (PBI-Py/PGO) applied in fuel cells [116]. The incorporation of 1.5 wt.% of PGO in the membrane attained the highest conductivity value of 76.4×10^{-3} S/cm at 140 °C (compared with 19.6×10^{-3} S/cm for PA doped PBI-Py membrane under similar conditions). In addition, the durability of the proton transport was significantly improved in the PGO containing membranes.

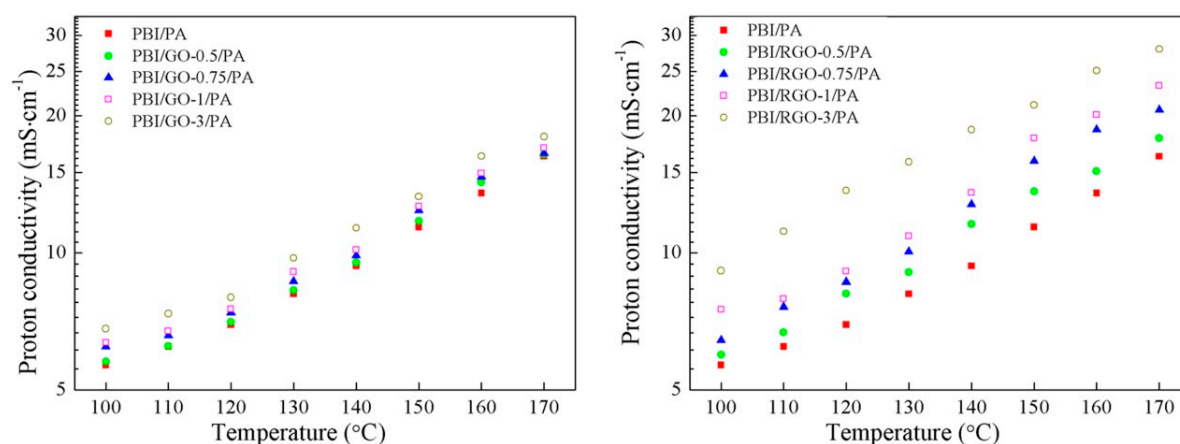


Figure 18. Temperature dependence of proton conductivity of PBI/GO/PA (left) and PBI/RGO/PA (right) membranes. Reproduced from [126] with permission of John Wiley and Sons.

Carbon nanotubes (CNTs) have been shown to be promising materials for various applications, such as biological and biomedical research [160,161], environmental science [162], catalysis [163], fabrication of composite materials [164], microelectronics [165], solar cells [166,167], electronic components [168,169], energy storage [170], hydrogen storage [171], and so on. The PBI-based composed membranes with CNTs (PBI/CNT) were investigated and their properties were compared with the plain PBI membrane. The proton conductivity of PA-doped PBI and PBI/CNT was 0.063 and 0.074 S/cm, respectively, at 180 °C [172].

Liu and co-workers prepared PBI-functionalized multiwalled carbon nanotubes (MWCNTs) through an ozone mediated process [173] and used as fillers in the preparation of PBI/MWCNT nanocomposite membranes [174]. In the preparation of PBI/MWCNT nanocomposite membranes using the conventional solution casting method, MWCNT/PBI were well dispersed in the PBI solution. Interestingly, the addition of the functionalized MWCNTs enhanced the thermal and mechanical properties of the composite membranes, increasing the Young's moduli and tensile strength 70% and 75%, respectively, with respect to pristine PBI membrane. Regarding the PA-doped PBI nanocomposite membrane containing 0.2 wt.% of MWCNT–PBI, it had a proton conductivity of 0.08 S/cm at 160 °C under anhydrous conditions, compared with the proton conductivity of 0.045 S/cm of the PA-doped PBI membrane (Figure 19). The authors attributed the high proton conductivity to the relatively high acid uptake level of PBI composite membranes and proton migration under anhydrous conditions was described to be mainly based on a Grotthuss-type mechanism. In studies of performance in single cell tests at 150 °C, the MWCNT/PBI composite membranes demonstrated maximum power densities of 600 mW/cm². These values are much higher than that found with a pristine PBI membrane (530 mW/cm²) and lower than that of MWCNT/Nafion[®] nanocomposite membranes containing the same amount of MWCNT, whose value was 700 mW/cm².

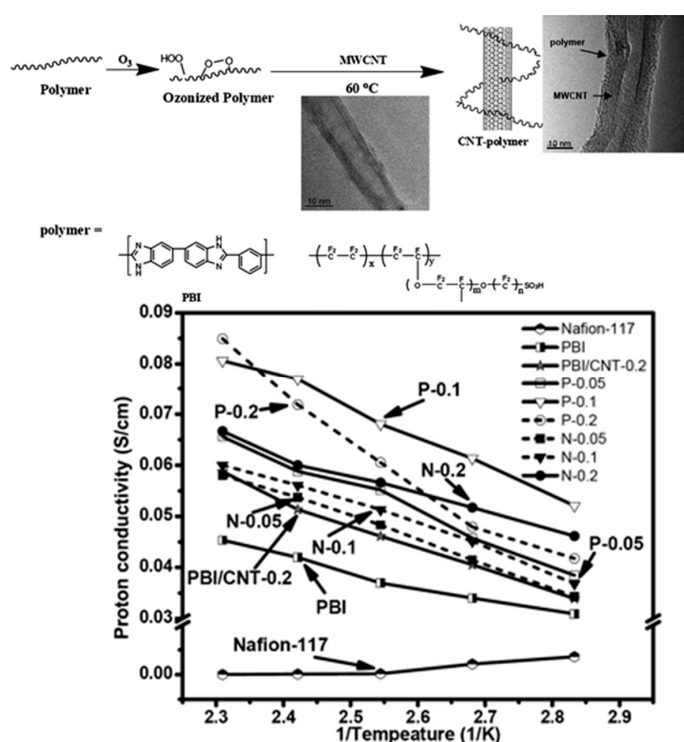


Figure 19. Schematic representation of preparation of sulfonated Nafion[®]- and PBI-functionalized multiwalled carbon nanotubes (MWCNTs) (top) and proton conductivity of different composite membranes at 80–160 °C without humidification (bottom). Reproduced from [174] with permission of the Royal Society of Chemistry.

Table 9. Composite membranes of polybenzimidazole derivatives with GO derivatives. MWCNT, multiwalled carbon nanotube. GO, graphene oxide; PGO, phosphonated GO; SGO, sulfonated GO; TrGO, GO bearing triazole groups.

Polymer	Filler	wt.%	σ_{DC} (S/cm)	T (°C)	PA	Ref
PBI	GO	2	0.170	165	—	[38]
PBI	TrGO	1.2	0.135	180	D	[159]
PBI	SGO	1	0.023	170	D	[126]
PBI-Py	PGO	1.5	0.076	140	D	[118]
PBI	CNT		0.074	180	D	[172]
PBI	MWCNT	0.2	0.08	160	D	[175]

On the other hand, the PBI nanocomposite membranes filled with phosphonate functionalized carbon nanotube (P-MWCNT) were also prepared and their properties were studied. It was shown that the two properties of key importance for PEM—the proton conductivity and mechanical stability above 100 °C—were improved [175]. It turned out that P-MWCNTs, being incorporated into the PA-doped PBI matrix, organized in domain-like structures. The enhanced performance was attributed to the formation of proton conducting networks that formed along the sidewalls of P-MWCNTs with a domain size of 17 nm.

In 2013, Hsu and co-workers prepared PBI composite membranes containing carbon nanotubes with different functional groups, which were studied for proton exchange membrane fuel cells [176]. Two approaches were employed in the functionalization of MWNTs. The first functionalization involved non-covalent modification by an in situ radical polymerization of sodium 4-vinylbenzenesulfonate with MWNTs to yield MWNT-poly (NaSS) [177]. The second approach involved the covalent modification of COOH-modified MWNTs by reaction with 1-(3-aminopropyl) imidazole through DCC-mediated amide bond formation to afford imidazole-functionalized MWNTs [178]. Next, composite membranes were prepared via the casting method using mixtures of functionalized MWNT and a fluorine containing PBI solution. The PBI composite membranes containing imidazole-functionalized MWNT provided more significant mechanical reinforcement compared with unmodified MWNTs and MWNT-poly (NaSS) membranes, which was attributed to its better compatibility with PBI. For PA doped MWNT-poly(NaSS)/PBI and MWNT-imidazole/PBI composite membranes, the proton conductivities were up to 0.051 and 0.043 S/cm at 160 °C under anhydrous condition, respectively, which were slightly higher than pristine PBI (0.028 S/cm). This enhancement was attributed to the combination of the increase of free volume of the membranes at higher temperatures and the positive correction between volume swelling and acid-doping level.

In 2015, Guerrero Moreno and co-workers prepared composite polymeric PBI membranes filled with 1 wt.% of MWCNTs (with 20 and 140 nm inner and outside diameter, respectively, and 8 μ m length) by spin coating [179]. The mechanical stability of the PBI membrane improved upon the addition of the carbon-based materials. The tensile strength of the composite PBI/CNT membrane with 1 wt.% CNTs loading was found to be 32% higher than the pristine PBI membrane. When studying the proton conductivity at 180 °C under anhydrous conditions, the PA doped PBI/MWCNT composite membrane exhibited a conductivity of 0.074 S/cm, slightly higher than that for the PA doped PBI membrane (0.063 S/cm). The authors attributed this enhancement to the higher molar ratio of PA to the polymer-repeat-unit owing to the presence of the CNTs.

5.3. Metal Organic Frameworks

Metal-organic structures (MOFs) are another type of commonly used filler used to improve proton conductivity in polymer electrolyte membranes. In recent years, the use of metal-organic structures as fillers in PEMs has attracted interest owing to their high conductivity, which is mainly attributed to their high porosity and the retention of water molecules in their pores [180–183]. The MOFs are a family of metal-based crystalline porous materials that contain bonding organic units,

which can form strong bonds, and lead to the creation of open crystalline structures with regular porous arrangement [184–186]. These interesting compounds have been studied for possible different applications such as fuel cells [187], pervaporation [188], nanofiltration [189], gas separation [190], desammonia adsorption [191], and organocatalysis [192]. The introduction of MOFs into organic polymer results in the enhanced thermal chemical stability of the formed composites under harsh conditions, making them suitable for industrial application [193]. For elaboration of these membranes, polymers such as perfluorosulfonic acid [194], sulfonated poly (ether ether ketone) [195], and poly(vinyl alcohol) [196] have been used.

As illustrated in Figure 20, the number of published research articles on MOF containing materials for fuel cell applications has increased significantly over the past decade, especially in recent years (2016–2019). Over the past decade, a diverse range of MOFs have been used as fillers in the preparation of mixed matrix membranes based on Nafion[®] [197–201], SPEEK [202–206], and other polymeric materials [207–211]; however, their use in PBI polymers is still very scarce.

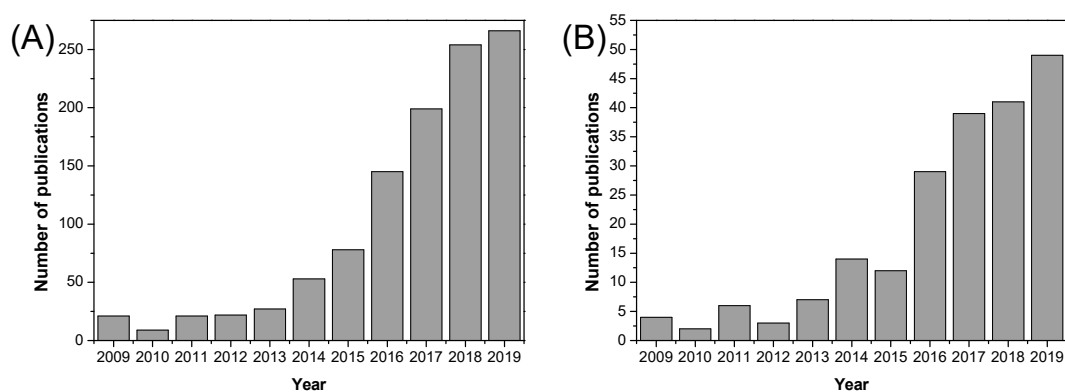


Figure 20. Number of publications in the period of 2009–2019 indexed in the Web of Science: (A) keywords: metal organic framework AND fuel cell; and (B) keywords: metal organic framework AND fuel cell AND proton exchange membrane. Source: www.webofknowledge.com.

In this regard, our group prepared PBI membranes containing the imidazolate zeolites (ZIFs) [77], a subclass of MOFs. ZIFs are materials with zeolitic topology when a M^{2+} tetrahedral divalent metal cation ($M = Co, Zn$) coordinates to four imidazolate rings, forming a neutral ($M(\text{Im})_2$) porous structure of high chemical and thermal stability [212,213]. The conductivity in the ZIF/PBI composite membranes containing 5 wt.% ZIF fillers varied from 0.003 to 0.091 S/cm at 200 °C, depending on the type of ZIF (Figure 21).

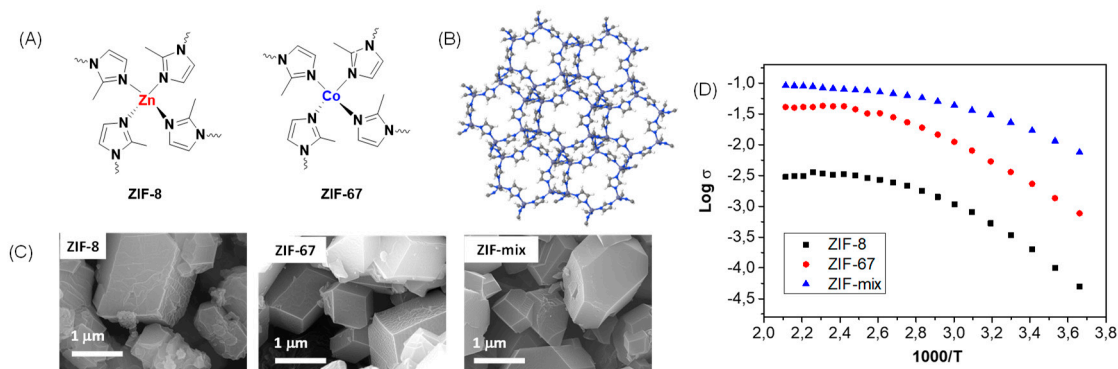


Figure 21. (A) Schematic representation of chemical structure of ZIF-8 and ZIF-69. (B) Structural representation of ZIF-8. (C) Field-emission scanning electron microscopy (FE-SEM) images of ZIF-8, ZI-67, and ZIF-mix. (D) Arrhenius plot of phosphoric acid doped PBI composite membranes containing 5 wt.% of ZIFs [77].

5.4. Ionic Liquids and Other Conductive Compounds

The use of ionic liquids (ILs) as conductive fillers to replace PA was proposed in an attempt to overcome the disadvantages of PA, such as leaching and conduction instability with the time mentioned above. ILs are purely ionic materials with generally low, below 100 °C, melting temperatures [214]. ILs have found applications in a wide variety of fields including their use as green solvents in organic synthesis [215], catalysis [216,217], extraction, separation [218], supramolecular chemistry [219,220], transport agents [221], pharmaceutical chemistry [222], materials science, and drug sensing [223], among others. ILs have several favorable properties including their temperature stability, non-volatility and non-flammability, rather high ionic conductivity, and reduced environmental impact. So, ILs are considered as promising compounds for the preparation of electrochemical devices [224]. As shown in Table 10, proton conductivity values close to 0.1 S/cm can be reached using ionic liquids as fillers in composite PBI membranes.

As shown in Figure 22, ionic liquids began to be used in fuel cells since their discovery at the beginning of the 21st century, and the number of publications of the use of ionic liquids in fuel cells has flourished in the past 15 years.

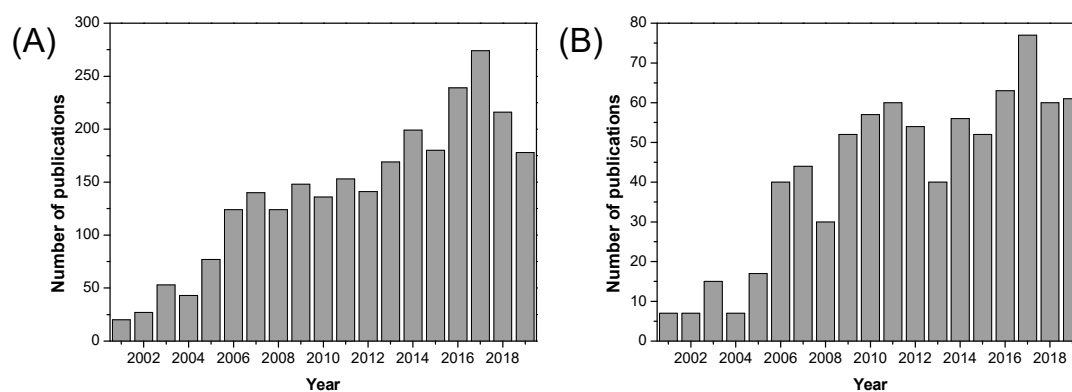


Figure 22. Number of publications in the period of 2001–2019 indexed in the Web of Science: (A) keywords: ionic liquid AND fuel cell; and (B) keywords: ionic liquid AND fuel cell AND proton exchange membrane. Source: www.webofknowledge.com.

Wang and coworkers prepared a polymer composite membrane based on fluorine containing PBI and 1-hexyl-3-methylimidazolium trifluoromethanesulfonate (HMI-Tf) as IL [225]. The conductivity of the PBI/HMI-Tf membrane was 0.016 S/cm at 250 °C under anhydrous conditions. Then, Ven and coworkers introduced 1-H-3-methylimidazolium bis(trifluoromethanesulfonyl)imide ([h-mim] Ntf₂) IL in the PBI support [226]. The resulting membrane showed a proton conductivity of 0.002 S/cm at 190 °C and the thermal stability in the range of 150–190 °C. Recently, our group prepared a series of PEMs based on PBI filled with 1-butyl-3-methylimidazolium (BMIM) bearing different anions (Cl, I, BF₄, PF₆, NCS, Br, NTf₂, BF₄) [227,228]. Under PA doping conditions, these composite membranes with 5 wt.% of ILs exhibited the highest proton conductivity of 0.098 S/cm at 120 °C when BF₄ anion was present.

Table 10. Composite membranes of polybenzimidazole with ionic liquids (ILs). HMI-Tf, 1-hexyl-3-methylimidazolium trifluoromethanesulfonate; BMIM, 1-butyl-3-methylimidazolium; SPAN, sulfonated polyaniline.

Polymer	ILs	wt.%	σ_{DC} (S/cm)	T (°C)	Ref
<i>o</i> -F ₆ -PBI	HMI-Tf	3	0.016	250	[225]
PBI	[h-mim] NTf ₂	—	0.00186	190	[226]
PBI	BMIM	5	0.098	120	[227]
PBI	Cl	5	1.0×10^{-4}	160	[227]
PBI	BF ₄	5	3×10^{-6}	160	[227]
PBI	NCS	5	4×10^{-7}	160	[227]
PBI	NTf ₂	5	6.5×10^{-4}	160	[227]
PBI	[dema][TfO] ₃₃	33	$<10^{-4}$	160	[229]
PBI	[dema][TfO] ₅₀	50	$<10^{-4}$	160	[229]
OPBI	perovskite (SrCeO ₃)-PA	8	0.105	180	[230]
PBI-TGIC (5%)	SPAN	50	0.13	180	[145]
PBI-TGIC (10%)	SPAN	50	0.12	180	[145]

Liu et al. [229] found that the membranes composed of PBI/[dema][TfO]₃₃ and PBI/[dema][TfO]₅₀ exhibited low conductivity ($<10^{-4}$ S/cm at 160 °C) at a low content of IL in the polymer matrix and reasonably high conductivity ($>10^{-3}$ S/cm at 40 °C) when the concentration of [dema][TfO] in the polymer increased to 83% (PBI/[dema][TfO]₈₃). The growth in conductivity at a higher IL content may be explained by enhanced free ionic mobility in the membrane matrix and the formation of well-developed ionic channels. The MEAs built with such composite membranes showed conductivity levels comparable to the data reported for other composite membranes, suggesting that the IL composite membranes have a potential for HT-PEMFC application under anhydrous conditions (Figure 23).

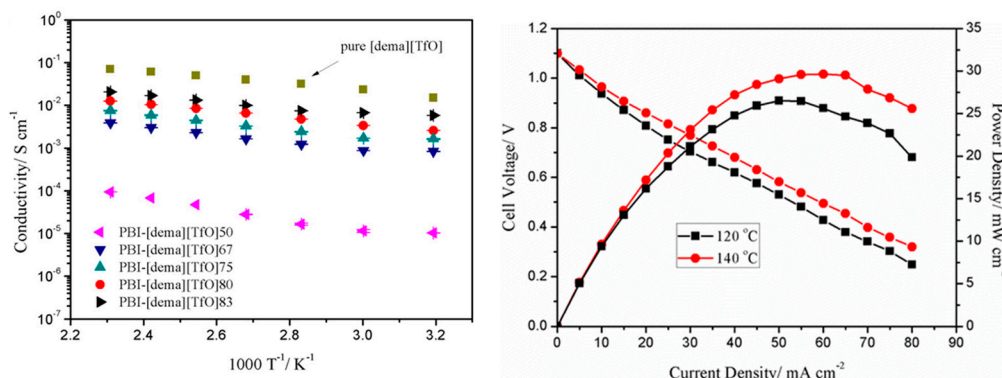


Figure 23. Variation of the conductivity of the ionic liquid (IL) and membranes at different temperatures (left) and polarization curve of an anhydrous H₂/Cl₂ fuel cell using the PBI/[dema][TfO]₈₃ composite membrane at different temperatures (right). Reproduced from [229] with permission of the American Chemical Society.

Xipeng Soing et al. [230] prepared a series of poly(oxyphenylene benzimidazole) (OPBI)/ionic liquid (IL) composite membranes mixing the polymer with 1-butyl-3-methylimidazolium tetrafluoroborate ([BMIm]BF₄). The obtained membranes had high proton selectivity that was useful for application as vanadium redox flow batteries. It was also found that, when the IL content increased, the vanadium resistance and proton conductivity of the membranes increased, obtaining an optimized proton selectivity for OPBI/BF₄-20 composite membrane. The optimum value was 1.41×10^6 S·min cm⁻³, which was much higher than that of the unmodified OPBI membrane (6.06×10^5 S·min cm⁻³) or a commercialized Nafion[®] 115 membrane (1.61×10^4 S·min cm⁻³). On the other hand, OPBI/BF₄-20 exhibited a higher coulombic efficiency (CE, 99.24%), voltage efficiency (VE, 93.10%), and energy

efficiency (EE, 92.39%) at 40 mA cm⁻² than the unmodified OPBI (CE 98.06%, VE 90.67%, and EE 88.86%) and even higher than Nafion[®] 115 membranes (CE 95.44%, VE 91.75%, and EE 87.57%).

Finally, studies carried out on the PBI-based membranes prepared by covalent crosslinking with triglycidylisocyanurate (TGIC) and doped with highly sulfonated polyaniline (SPAN) showed the good thermal, dimensional, mechanical, and oxidative stability of these membranes applied in MEAs of direct methanol fuel cells (DMFCs) [231]. The relatively low degree of cross-linking allowed high doping level of SPAN and, consequently, the high proton conductivity. The proton conductivities of PBI-TGIC (5%)/SPAN(50%) and PBI-TGIC(10%)/SPAN (50%) were 0.13 and 0.12 S/cm, respectively, at 180 °C and 100% RH; 0.064 and 0.058 S/cm, respectively, at 180 °C and 50% RH; and 0.018 and 0.016 S/cm, respectively, at 180 °C and 0% RH.

5.5. Electrospun Fillers

Among the different approaches to develop novel materials in the fabrication of PEMFC for sustainable energy devices, nanofibrous structured materials have become an efficient alternative in the midst of several fuel concerns. As displayed in Figure 24, the number of publications concerning nanofibrous materials for fuel cell applications is still growing.

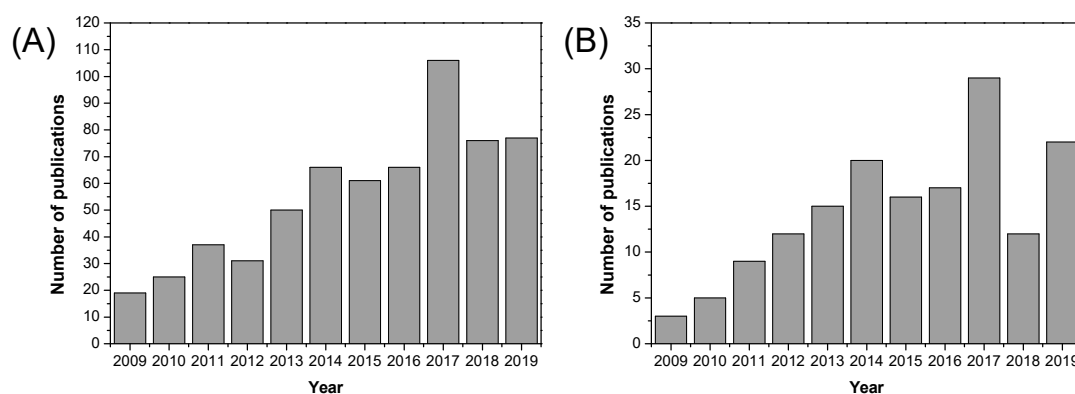


Figure 24. Number of publications in the period of 2009–2019 indexed in the Web of Science: (A) keywords: electrospinning AND fuel cell; and (B) keywords: electrospinning AND fuel cell AND proton exchange membrane. Source: www.webofknowledge.com.

Electrospinning has generated considerable interest as a promising method for fabricating nanofiber-based PEMs owing to the specific properties associated with its advanced features, including the high surface area, low density, high porosity, fully interconnected pores, high orientation or alignment of nanofibers, and easy scalability.

PEMs composed of aligned electrospun nanofibers can offer a uniaxial arrangement of the polymer chains in nanofibers, thereby providing better mechanical properties and promoting the formation of interconnected channels, resulting in enhanced proton conductivity [232]. In the field of PEMs, polymers such as sulfonated poly (ether ether ketone) [233,234], polyimide [235], and Nafion[®] [236,237], among others, have been electrospun into fibers.

Li and coworkers prepared polybenzoxazine (PBz)-modified polybenzimidazole (PBI) nanofibers by the electrospinning process [238]. The nanofibers were crosslinked through the ring-opening addition reaction of the benzoxazine groups. Modification of the PBI composite membranes with the crosslinking PBI nanofibers significantly improves their mechanical properties, acid uptakes, and dimensional stability upon acid doping. The composite membranes showed proton conductivity of 0.17 S/cm at 160 °C under anhydrous conditions, which was about twofold higher than the proton conductivity of the neat PBI membrane. Muthuraja and coworkers prepared different types of membranes from the whole poly (aryl sulfone ether benzimidazole) (SO₂-OPBI) and from its nanofibers obtained by the electrospinning process [239]. Compared with the traditional PBI, presence of the sulfone and

ether linked in the polymeric backbones improved the membrane flexibility and its resistance towards radical oxidation, as noted above. Nanofiber SO_2 -OPBI membrane reached proton conductivity of 0.067 S/cm, which was higher than that of dense SO_2 -OPBI (0.033 S/cm) and PBI membranes (0.008 S/cm) at 160 °C. As a result, the acid doped SO_2 -OPBI membranes showed better chemical strength and higher proton conductivity.

Jahangiri and coworkers produced PBI electrospun nanofiber of 170 nm diameter [240]. Immersion into PA for 72 h led to a highest proton conductivity of 0.123 S/cm, whereas the conductivity of 96 h doped PBI mats decreased. Tensile strength of the membranes was found to increase with doping level, whereas the strain at break (%) decreased because of the brittle nature of the formed network (Figure 25).

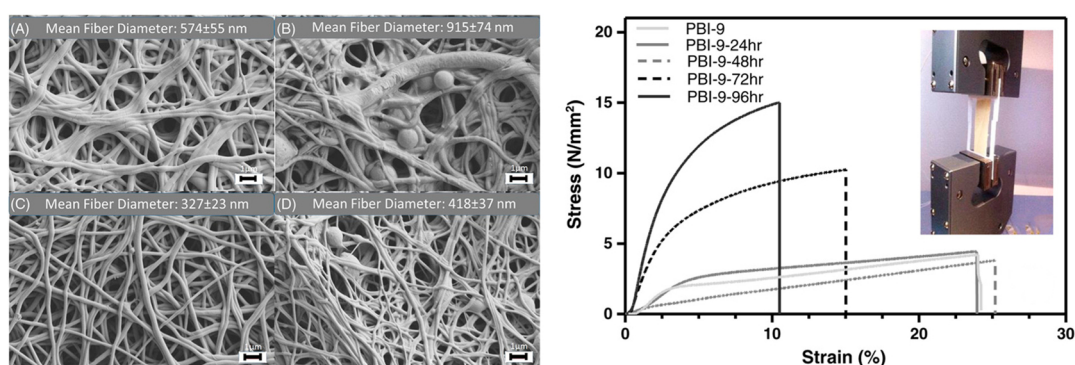


Figure 25. (Left) Scanning electron microscope micrographs of (A) PBI-9-24 h, (B) PBI-9-48 h, (C) PBI-9-72 h, and (D) PBI-9-96 h phosphoric acid-doped polybenzimidazole (PBI) nanofibers and (right) stress-strain curves of undoped and PA doped during 24, 48, 72, and 96 h electrospun membranes. Reproduced from [240] with permission of John Wiley and Sons.

Our group has also contributed to the field of nanofiber materials through the preparation of PBI composite membranes containing SiO_2 nanofiber mats [76]. The nanofiber materials were fabricated via the electrospinning process and later functionalized with terminal neutral, acidic, and basic groups using silane chemistry. This surface functionalization was characterized by X-ray photoelectron spectroscopy (XPS), which is a widely used surface characterization technique [241–243]. The different functionalized nanofiber mats were embedded into a PBI matrix to fabricate composite membranes with enhanced chemical and thermal stability. Among the diverse composite membranes, those containing nanofibers with basic groups displayed higher conductivity with values up to 0.003 S/cm at 200 °C without phosphoric acid doping (Figure 26). As shown in Table 11, these membranes displayed lower conductivity than the previously reported membranes as they were used in undoped conditions.

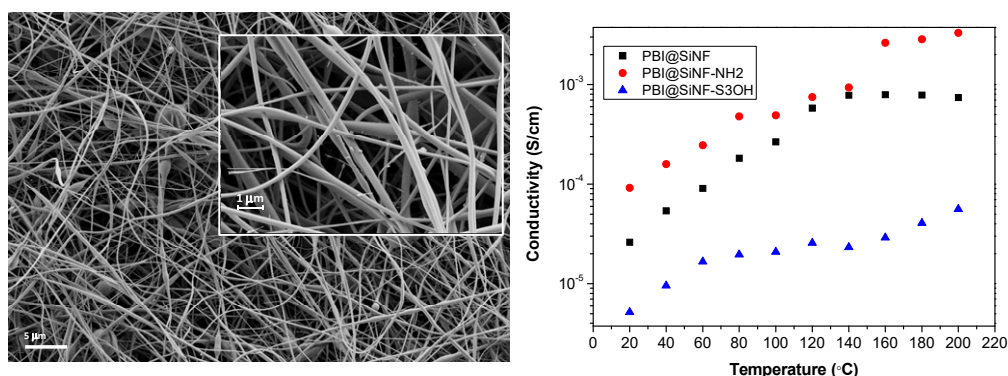


Figure 26. FE-SEM images of SiO_2 nanofibers and temperature dependence of composite PBI membranes with neutral (PBI@SiNF), basic (PBI@SiNF- NH_2), and acidic groups (PBI@SiNF- SO_3H) [76].

Table 11. Nanofibers polybenzimidazole derivatives.

Polymer	σ_{DC} (S/cm)	T (°C)	PA	Ref
PBI	0.123	200	D	[240]
SO ₂ -OPBI	0.067	160	D	[239]
m-PBI-PBz	0.170	160	D	[238]
PBI-basic SO ₂	0.003	200	—	[70]

6. Conclusions

In this review, an extensive outlook of the recent developments on composite membranes based on PBI for HT-PEMFC applications is given. The most common approach to increase proton conductivity in PBI membranes is based on the phosphoric acid doping, which enhances proton conductivity of these polymeric membranes up to 0.2 S/cm. However, degradation of the membrane at high temperatures and acid leaching are drawbacks that hamper their use as HT-PEMFCs. The use of alternatives based on the addition of fillers into the polymeric matrix can help to overcome these problems. As shown, proton conductivity values close to those of the commercially used Nafion[®] membranes can be reached using a wide diversity of materials used as fillers in PBI membranes. These fillers include carbon-based materials such as graphene oxide and carbon nanotubes, nanofibers obtained by electrospinning methods, inorganic fillers such as metal oxides and heteropolyacids, and organic fillers such as ionic liquids or metal organic frameworks. Other alternatives are based on the modification of PBI structure by synthetic methods or co-polymerization strategies, which can increase the proton conductivity and retain phosphoric acid more efficiently. Despite that high conductivities have been reported by these methods, phosphoric acid leaching remains a problem to be solved in the next decade.

Fuel cell technology is currently receiving much attention from researchers as well as from the industry because it can reduce the costs of the organic and inorganic fillers such as metal organic frameworks, ionic liquids, nanofibers, and carbon-based materials. The introduction of inorganic fillers into the polymer matrix of PBI in order to form novel composite membranes was reported to improve the dimensional stability, mechanical properties, and gas permeability of PBI composite membranes.

The effective design of composite membranes based-PBI doped with phosphoric acid for high performance PEMs for fuel cells has been demonstrated with higher performance and durability. The composite membranes based on PBI formed with nanofibers and organic and inorganic fillers show good mechanical properties and solvent-resistance, proving the latter to be effective additives for the preparation of reinforced PBI composite membranes through a solution process enhancing the formation of long-range proton-conductive pathways in the PBI membranes. The acid-uptake levels, dimensional stability upon acid-doping, and proton conductivity of the PBI-based membranes through retention of phosphoric acid have been significantly enhanced by the formation of composite membranes with cross-linked PBI. Cross-linking plays an important role in forming additional networks in PBI, despite that it generally weakens the interaction between the filler and polymer chain; however, cross-linking reinforces the polymer chain with additives producing more novel rigid materials. On the other hand, plasticizers can form composites membranes with high flexibility, reducing hydrophilic or hydrophobic properties (depending on the nature of the plasticizers), and even increasing the proton conductivity. The addition of plasticizers has also increased the amorphous phase in PBI composites.

The use of additives involves a wide variety of technologies in polymer technology, with a great field of materials engineering to be applied in energy existing today. The focus of this review has been the use of additives in PBI membranes to facilitate PA doping to be durable over prolonged cyclic usage and, in the long term, especially to obtain high performance and durability in HT-PEMFC with low costs. The reported membranes have been studied from their physical structure and morphology as well as their chemical and electrochemical performance. As per our findings, most of the previous work found in the literature reported that the presence of additive material in a polymer matrix enhances the properties compared with the neat polymer. However, most of the synthesized membranes display poor performance in a single fuel cell in the presence of additives with a diminution in terms of proton

conductivity and mechanical strength owing to some problems such as the agglomeration, swelling, and interaction filler polymeric PBI matrix, among others. Consequently, there is a strong need to overcome these drawbacks and reach an equilibrium between proton conductivity and thermal and mechanical stability in the composite membrane.

The challenges and opportunities of composite membranes of PBI are still growing as their impact on the research and development (R&D) industry is under continuous growth, as the demand increases every year following that of devices operating at moderate and high temperatures. Thus, the design of novel materials is of crucial interest when providing major durability and strength of PBI. However, a crucial requirement they need to fulfill to be applied as fuel cells and as super capacitors is the need for high conductivity and long-term durability. For this purpose, as mentioned above, the use of PA doped membranes can be a strong limitation and, at the same time, an advantage, if the natural route is applied when synthesizing the additive. Nonetheless, there are still some aspects that need to be improved on these composite membranes based on PBI, such as reducing the degradation rates of the polymeric membranes present owing to the operation at high temperatures. It is also desirable to design new PEMs with enhanced chemical stability towards peroxide and radical attacks, as well as increase the retention factor of phosphoric acid to reduce the loss of the electrolyte, and maintain the proton conductivity for extended periods of time.

The market for polymer electrolyte membrane fuel cells is expected to grow at a compound annual growth rate (CAGR) of 15.28% during the next five years. Major factors driving the market are increasing R&D activities for energy applications, which has driven to various technological advantages, such as high power density, decrease in the time to refuel, longer storage durability, and increase of life-cycles of PEM fuel cells over alternatives such as Li-ion batteries; in addition, efforts have been focused on the design of PEM fuel cell-powered vehicles with the help of government incentives and policies. However, the current cost of PEMFC technology is still relatively high, a substantial limitation to overcome. In the next years, attempts have to be oriented towards getting around this important barrier, which can help to successfully implement this green technology in commercial usage for stationary and transportation, among others [244].

In the past few years, considerable progress has been made through the commercialization of HT-PEMFC technology, and it has emerged as an attractive alternative to other kinds. As an example, commercially available Advent PBI MEAs, based on PBI, possess excellent thermal and oxidative stability, and can operate at 120 to 180 °C using phosphoric acid as the electrolyte. Among the advantages, it is worth mentioning that they do not need water for conductivity and can reach proton conductivities up to 0.1 S/cm with a proven lifetime of 20,000 h [245]. The elevated operating temperature leads to important advantages, making them potential candidates as a near-future environmentally friendly technology.

Author Contributions: Conceptualization, J.E. and V.C.; formal analysis, J.E., J.O.-M., L.A., L.F.d.C. and V.C.; funding acquisition, V.C.; investigation, J.E., J.O.-M., L.A., L.F.d.C. and V.C.; methodology, J.E., J.O.-M., L.A., L.F.d.C. and V.C.; project administration, V.C.; supervision, J.E. and V.C.; validation, writing—original draft, J.E., J.O.-M., L.A., L.F.d.C. and V.C.; writing—review and editing, J.E., J.O.-M., L.A., L.F.d.C. and V.C. All authors have read, critically review and agreed to the published version of the manuscript.

Funding: The authors acknowledge the Spanish Ministerio de Economía y Competitividad (MINECO) for the financial support under the project ENE/2015-69203-R.

Acknowledgments: The authors kindly thank Jordi Salinas from Universidad Nacional Autónoma de México for the English style revision.

Conflicts of Interest: The authors declare no conflict of interest.

References

1. Kreuer, K.D.; Paddison, S.J.; Spohr, E.; Schuster, M. Transport in Proton Conductors for Fuel-Cell Applications: Simulations, Elementary Reactions, and Phenomenology. *Chem. Rev.* **2004**, *104*, 4637–4678. [[CrossRef](#)]
2. Hammes-Schiffer, S.; Soudackov, A.V. Proton-Coupled Electron Transfer in Solution, Proteins, and Electrochemistry. *J. Phys. Chem. B* **2008**, *112*, 14108–14123. [[CrossRef](#)] [[PubMed](#)]
3. Kraysberg, A.; Ein-Eli, Y. Review of Advanced Materials for Proton Exchange Membrane Fuel Cells. *Energy Fuels* **2014**, *28*, 7303–7330. [[CrossRef](#)]
4. Li, Q.; Jensen, J.O.; Savinell, R.F.; Bjerrum, N.J. High temperature proton exchange membranes based on polybenzimidazoles for fuel cells. *Prog. Polym. Sci.* **2009**, *34*, 449–477. [[CrossRef](#)]
5. Cleghorn, S.J.C.; Springer, T.E.; Wilson, M.S.; Zawodzinski, C.; Zawodzinski, T.A.; Gottesfeld, S. PEM fuel cells for transportation and stationary power generation applications. *Int. J. Hydrog. Energy* **1997**, *22*, 1137–1144. [[CrossRef](#)]
6. Scott, K.; Shukla, A.K. Polymer electrolyte membrane fuel cells: Principle and advances. *Rev. Environ. Sci. Bio/Technol.* **2004**, *3*, 273–280. [[CrossRef](#)]
7. Whittingham, M.S.; Savinell, R.F.; Zawodzinski, T. Introduction: Batteries and Fuel Cells. *Chem. Rev.* **2004**, *104*, 4243–4244. [[CrossRef](#)]
8. Zhang, H.; Shen, P.K. Recent Development of Polymer Electrolyte Membranes for Fuel Cells. *Chem. Rev.* **2012**, *112*, 2780–2832. [[CrossRef](#)]
9. Cano, Z.P.; Banham, D.; Ye, S.; Hintennach, A.; Lu, J.; Fowler, M.; Chen, Z. Batteries and fuel cells for emerging electric vehicle markets. *Nat. Energy* **2018**, *3*, 279–289. [[CrossRef](#)]
10. Campanari, S.; Manzolini, G.; García de la Iglesia, F. Energy analysis of electric vehicles using batteries or fuel cells through well-to-wheel driving cycle simulations. *J. Power Sources* **2009**, *186*, 464–477. [[CrossRef](#)]
11. Merle, G.; Wessling, M.; Nijmeijer, K. Anion exchange membranes for alkaline fuel cells: A review. *J. Membr. Sci.* **2011**, *377*, 1–35. [[CrossRef](#)]
12. Wasmus, S.; Küver, A. Methanol oxidation and direct methanol fuel cells: A selective review. *J. Electroanal. Chem.* **1999**, *461*, 14–31. [[CrossRef](#)]
13. Wang, Y.; Chen, K.S.; Mishler, J.; Cho, S.C.; Cordobes Adrohe, X.C. A review of polymer electrolyte membrane fuel cells: Technology, applications, and needs on fundamental research. *Appl. Energy* **2011**, *88*, 981–1007. [[CrossRef](#)]
14. Choudhury, S.R. Phosphoric Acid Fuel Cell Technology. In *Recent Trends in Fuel Cell Science and Technology*; Basu, S., Ed.; Springer: New York, NY, USA, 2007.
15. Watanabe, T. Molten Carbonate Fuel Cells. In *Handbook of Climate Change Mitigation*; Chen, W.Y., Seiner, J., Suzuki, T., Lackner, M., Eds.; Springer: New York, NY, USA, 2012.
16. Ormerod, R.M. Solid oxide fuel cells. *Chem. Soc. Rev.* **2003**, *32*, 17–28. [[CrossRef](#)]
17. Dresch, S.; Luo, F.; Schmack, R.; Kühl, S.; Gliech, M.; Strasser, P. An efficient bifunctional two-component catalyst for oxygen reduction and oxygen evolution in reversible fuel cells, electrolyzers and rechargeable air electrodes. *Energy Environ. Sci.* **2016**, *9*, 2020–2024. [[CrossRef](#)]
18. Haile, S.M.; Boysen, D.A.; Chisholm, C.R.I.; Merle, R.B. Solid acids as fuel cell electrolytes. *Nature* **2001**, *410*, 910–913. [[CrossRef](#)]
19. Pourcelly, G. Membranes for low and medium temperature fuel cells. State-of-the-art and new trends. *Pet. Chem.* **2011**, *51*, 480–491. [[CrossRef](#)]
20. Scott, K.; Xu, C.X.; Wu, X. Intermediate temperature proton-conducting membrane electrolytes for fuel cells. *Wiley Interdiscip. Rev. Energy Environ.* **2014**, *3*, 24–41. [[CrossRef](#)]
21. Dupuis, A.-C. Proton exchange membranes for fuel cells operated at medium temperatures: Materials and experimental techniques. *Prog. Mater. Sci.* **2011**, *56*, 289–327. [[CrossRef](#)]
22. Park, C.H.; Lee, C.H.; Guiver, M.D.; Lee, Y.M. Sulfonated hydrocarbon membranes for medium-temperature and low-humidity proton exchange membrane fuel cells (PEMFCs). *Prog. Polym. Sci.* **2011**, *36*, 1443–1498. [[CrossRef](#)]
23. Sun, X.; Simonsen, S.C.; Norby, T.; Chatzidakis, A. Composite Membranes for High Temperature PEM Fuel Cells and Electrolysers: A Critical Review. *Membranes* **2019**, *9*, 83. [[CrossRef](#)] [[PubMed](#)]

24. Lee, K.-S.; Maurya, S.; Kim, Y.S.; Kreller, C.R.; Wilson, M.S.; Larsen, D.; Elangovan, S.E.; Mukundan, R. Intermediate temperature fuel cells via an ion-pair coordinated polymer electrolyte. *Energy Environ. Sci.* **2018**, *11*, 979–987. [[CrossRef](#)]
25. Mauritz, K.A.; Moore, R.B. State of Understanding of Nafion. *Chem. Rev.* **2004**, *104*, 4535–4585. [[CrossRef](#)] [[PubMed](#)]
26. Casciola, M.; Alberti, G.; Sganappa, M.; Narducci, R. On the decay of Nafion proton conductivity at high temperature and relative humidity. *J. Power Sources* **2006**, *162*, 141–145. [[CrossRef](#)]
27. Alberti, A.; Narducci, R.; Di Vona, M.L.; Giancola, S. More on Nafion Conductivity Decay at Temperatures Higher than 80 °C: Preparation and First Characterization of In-Plane Oriented Layered Morphologies. *Ind. Eng. Chem. Res.* **2013**, *52*, 10418–10424. [[CrossRef](#)]
28. Li, Q.F.; He, R.H.; Jensen, J.O.; Bjerrum, N.J. Approaches and Recent Development of Polymer Electrolyte Membranes for Fuel Cells Operating above 100 °C. *Chem. Mater.* **2003**, *15*, 4896–4915. [[CrossRef](#)]
29. Alberti, G.; Narducci, R.; Sganappa, M. Effects of hydrothermal/thermal treatments on the water-uptake of Nafion membranes and relations with changes of conformation, counter-elastic force and tensile modulus of the matrix. *J. Power Sources* **2008**, *178*, 575–583. [[CrossRef](#)]
30. Subianto, S.; Choudhury, N.R.; Dutta, N. Composite Electrolyte Membranes from Partially Fluorinated Polymer and Hyperbranched, Sulfonated Polysulfone. *Nanomaterials* **2014**, *4*, 1–18. [[CrossRef](#)]
31. Zhang, J.; Xie, Z.; Zhang, J.; Tang, Y.; Song, C.; Navessin, T.; Shi, Z.; Song, D.; Wang, H.; Wilkinson, D.P.; et al. High temperature PEM fuel cells. *J. Power Sources* **2006**, *160*, 872–891. [[CrossRef](#)]
32. Neburchilov, V.; Martin, J.; Wan, H.; Zhang, J. A review of polymer electrolyte membranes for direct methanol fuel cells. *J. Power Sources* **2007**, *169*, 221–238. [[CrossRef](#)]
33. Zeis, R. Materials and characterization techniques for high-temperature polymer electrolyte membrane fuel cells. *Beilstein J. Nanotechnol.* **2015**, *6*, 68–83. [[CrossRef](#)] [[PubMed](#)]
34. Rasheed, R.K.A.; Liao, Q.; Zhang, C.; Chan, S.H. A review on modelling of high temperature proton exchange membrane fuel cells (HT-PEMFCs). *Int. J. Hydrog. Energy* **2017**, *42*, 3142–3165. [[CrossRef](#)]
35. Rikakawa, M.; Sanui, K. Proton-conducting polymer electrolyte membranes based on hydrocarbon polymers. *Prog. Polym. Sci.* **2000**, *25*, 1463–1502. [[CrossRef](#)]
36. Kurdakova, V.; Quartarone, E.; Mustarelli, P.; Magistris, A.; Caponetti, E.; Saladino, M.L. PBI-based composite membranes for polymer fuel cells. *J. Power Sources* **2010**, *195*, 7765–7769. [[CrossRef](#)]
37. Wang, S.; Zhang, G.; Han, M.; Li, H.; Zhang, Y.; Ni, J.; Ma, W.; Li, M.; Wang, J.; Liu, Z.; et al. Novel epoxy-based cross-linked polybenzimidazole for high temperature proton exchange membrane fuel cells. *Int. J. Hydrog. Energy* **2011**, *36*, 8412–8421. [[CrossRef](#)]
38. Üregen, N.; Pehlivanoglu, K.; Özdemir, Y.; Devrim, Y. Development of polybenzimidazole/graphene oxide composite membranes for high temperature PEM fuel cells. *Int. J. Hydrog. Energy* **2017**, *42*, 2636–2647. [[CrossRef](#)]
39. Lipman, T.E.; Edwards, J.L.; Kammen, D.M. Fuel cell system economics: Comparing the costs of generating power with stationary and motor vehicle PEM fuel cell systems. *Energy Policy* **2004**, *32*, 101–125. [[CrossRef](#)]
40. Savinell, R.; Yeager, E.; Tryk, D.; Landau, U.; Wainright, J.; Weng, D.; Lux, K.; Litt, M.; Roger, C. A Polymer Electrolyte for Operation at Temperatures up to 200 °C. *J. Electrochem. Soc.* **1994**, *141*, L46–L48. [[CrossRef](#)]
41. Wainright, J.S.; Wang, J.T.; Weng, D.; Savinell, R.F.; Litt, M. Acid-Doped Polybenzimidazoles: A New Polymer Electrolyte. *J. Electrochem. Soc.* **1995**, *142*, L121–L123. [[CrossRef](#)]
42. Li, Q.; He, R.; Jensen, J.O.; Bjerrum, N.J. PBI-Based Polymer Membranes for High Temperature Fuel Cells—Preparation, Characterization and Fuel Cell Demonstration. *Fuel Cells* **2004**, *4*, 147–159. [[CrossRef](#)]
43. Asensio, J.A.; Sanchez, E.M.; Gomez-Romero, P. Proton-conducting membranes based on benzimidazole polymers for high-temperature PEM fuel cells. *A Chem. Quest. Chem. Soc. Rev.* **2010**, *39*, 3210–3239. [[CrossRef](#)] [[PubMed](#)]
44. Araya, S.S.; Zhou, F.; Liso, V.; Sahlin, S.L.; Vang, J.R.; Thomas, S.; Gao, X.; Jeppesen, C.; Kaer, S.K. A comprehensive review of PBI-based high temperature PEM fuel cells. *Int. J. Hydrog. Energy* **2016**, *41*, 21310–21344. [[CrossRef](#)]
45. Vogel, H.; Marvel, S. Polybenzimidazoles, new thermally stable polymers. *J. Polym. Sci.* **1961**, *50*, 511–539. [[CrossRef](#)]
46. Buckley, A.; Stuetz, D.E.; Serad, G.A. *Encyclopedia of Polymer Science and Engineering*; J. Wiley & Sons: New York, NY, USA, 1986; Volume 11, pp. 572–601.

47. Choe, E.W.; Choe, D.D. *Polymeric Materials Encyclopedia*; CRC Press: Boca Raton, FL, USA, 1996; Volume 7, pp. 5619–5637.
48. Mack, F.; Klages, M.; Scholta, J.; Jörisen, L.; Morawietz, T.; Hiesgen, R.; Kramer, D.; Zeis, R. Morphology studies on high-temperature polymer electrolyte membrane fuel cell electrodes. *J. Power Sources* **2014**, *255*, 431–438. [[CrossRef](#)]
49. Perry, K.A.; More, K.L.; Payzant, E.A.; Meisner, R.A.; Sumpter, B.G.; Benicewicz, B.C. A comparative study of phosphoric acid-doped m-PBI membranes. *J. Polym. Sci. Part. B* **2014**, *52*, 26–35. [[CrossRef](#)]
50. Quartarone, E.; Angioni, S.; Mustarelli, P. Polymer and Composite Membranes for Proton-Conducting, High-Temperature Fuel Cells: A Critical Review. *Materials* **2017**, *10*, 687. [[CrossRef](#)]
51. Kirubakaran, A.; Jain, S.; Nema, R.K. A review on fuel cell technologies and power electronic interface. *Renew. Sustain. Energy Rev.* **2009**, *13*, 2430–2440. [[CrossRef](#)]
52. Ponomarev, I.I.; Goryunov, E.I.; Petrovskii, P.V.; Ponomarev, I.I.; Volkova, Y.A.; Razorenov, D.Y. Synthesis of new monomer 3,3'-diamino-4,4'-bis[p-[(diethoxyphosphoryl)methyl]phenylamino]diphenyl sulfone and polybenzimidazoles on its basis. *Dokl. Chem.* **2009**, *429*, 315–320. [[CrossRef](#)]
53. Feifei, N.G.; Peron, J.; Jones, D.J.; Roziere, J. Synthesis of novel proton-conducting highly sulfonated polybenzimidazoles for PEMFC and the effect of the type of bisphenyl bridge on polymer and membrane properties. *J. Polym. Sci. Part A Polym. Chem.* **2011**, *49*, 2107–2117.
54. Carollo, A.; Quartarone, E.; Tomasi, C.; Mustarelli, P.; Belotti, F.; Magistris, A.; Maestroni, F.; Parachini, M.; Garlaschelli, L.; Righetti, P.P. Developments of new proton conducting membranes based on different polybenzimidazole structures for fuel cells applications. *J. Power Sources* **2006**, *160*, 175–180. [[CrossRef](#)]
55. Mustarelli, P.; Quartarone, E.; Grandi, S.; Angioni, S.; Magistris, A. Increasing the permanent conductivity of PBI membranes for HT-PEMs. *Solid State Ion.* **2012**, *225*, 228–231. [[CrossRef](#)]
56. Conti, F.; Majerus, A.; Di Noto, V.; Korte, C.; Lehnert, W.; Stolten, D. Raman study of the polybenzimidazole-phosphoric acid interactions in membranes for fuel cells. *Phys. Chem. Chem. Phys.* **2012**, *14*, 10022–10026. [[CrossRef](#)]
57. Wippermann, K.; Wannek, C.; Oetjen, H.-F.; Mergel, J.; Lehnert, W. Cell resistances of poly(2,5-benzimidazole)-based high temperature polymer membrane fuel cell membrane electrode assemblies: Time dependence and influence of operating parameters. *J. Power Sources* **2010**, *195*, 2806–2809. [[CrossRef](#)]
58. Mack, F.; Aniol, K.; Ellwein, C.; Kerres, J.; Zeis, R. Novel phosphoric acid-doped PBI-blends as membranes for high-temperature PEM fuel cells. *J. Mater. Chem. A* **2015**, *3*, 10864–10874. [[CrossRef](#)]
59. Li, Z.; He, G.; Zhang, B.; Cao, Y.; Wu, H.; Jiang, Z.; Tiantian, Z. Enhanced proton conductivity of Nafion hybrid membrane under different humidities by incorporating metal-organic frameworks with high phytic acid loading. *ACS Appl. Mater. Interfaces* **2014**, *6*, 9799–9807. [[CrossRef](#)]
60. Zhou, Y.; Yang, J.; Su, H.; Zeng, J.; Jiang, S.P.; Goddard, W.A. Insight into proton transfer in phosphotungstic acid functionalized mesoporous silica-based proton exchange membrane fuel cells. *J. Am. Chem. Soc.* **2014**, *136*, 4954–4964. [[CrossRef](#)] [[PubMed](#)]
61. Zeng, J.; Zhou, Y.; Li, L.; Jiang, S.P. Phosphotungstic acid functionalized silica nanocomposites with tunable bicontinuous mesoporous structure and superior proton conductivity and stability for fuel cells. *Phys. Chem. Chem. Phys.* **2011**, *13*, 10249–10257. [[CrossRef](#)]
62. Liu, X.; Li, Y.; Xue, J.; Zhu, W.; Zhang, J.; Yin, Y.; Qin, Y.; Jiao, K.; Du, Q.; Cheng, B.; et al. Magnetic field alignment of stable proton-conducting channels in an electrolyte membrane. *Nat. Commun.* **2019**, *10*, 842. [[CrossRef](#)]
63. Zhai, L.; Li, H. Polyoxometalate-Polymer Hybrid Materials as Proton Exchange Membranes for Fuel Cell Applications. *Molecules* **2019**, *24*, 3425. [[CrossRef](#)]
64. Escorihuela, J.; García-Bernabé, A.; Compañ, V. A Deep Insight into Different Acidic Additives as Doping Agents for Enhancing Proton Conductivity on Polybenzimidazole Membranes. *Polymers* **2020**, *12*, 1374. [[CrossRef](#)]
65. Yang, J.S.; Cleemann, L.N.; Steenberg, T.; Terkelsen, C.; Li, Q.F.; Jensen, J.O.; Hjuler, H.A.; Bjerrum, N.J.; He, R.H. High Molecular Weight Polybenzimidazole Membranes for High Temperature PEMFC. *Fuel Cells* **2014**, *14*, 7–15. [[CrossRef](#)]
66. Chaudhari, H.D.; Illathvalappil, R.; Kurungot, S.; Kharul, U.K. Preparation and investigations of ABPBI membrane for HT-PEMFC by immersion precipitation method. *J. Membr. Sci.* **2018**, *5*, 211–217. [[CrossRef](#)]

67. Shigematsu, A.; Yamada, T.; Kitagawa, H. Wide control of proton conductivity in porous coordination polymers. *J. Am. Chem. Soc.* **2011**, *133*, 2034–2036. [[CrossRef](#)] [[PubMed](#)]
68. De Grotthuss, C.J.T. Sur la décomposition de l'eau et des corps qu'elle tient en dissolution à l'aide de l'électricité galvanique. *Ann. Chim.* **1806**, *58*, 54–73.
69. Agmon, N. The Grotthuss Mechanism. *Chem. Phys. Lett.* **1995**, *244*, 456–462. [[CrossRef](#)]
70. Kreuer, K.-D.; Rabenau, A.; Weppner, W. Vehicle Mechanism, A New Model for the Interpretation of the Conductivity of Fast Proton Conductors. *Angew. Chem. Int. Ed.* **1982**, *21*, 208–209.
71. Bouchet, R.; Siebert, E. Proton conduction in acid doped polybenzimidazole. *Solid State Ion.* **1999**, *118*, 287–299. [[CrossRef](#)]
72. Gebbie, M.A.; Smith, A.M.; Dobbs, H.A.; Lee, A.A.; Warr, G.G.; Banquy, X.; Valtiner, M.; Rutland, M.W.; Israelachvili, J.N.; Perkin, S.; et al. Long range electrostatic forces in ionic liquids. *Chem. Commun.* **2017**, *53*, 1214–1224. [[CrossRef](#)]
73. Weingärtner, H. Understanding ionic liquids at the molecular level: Facts, problems, and controversies. *Angew. Chem. Int. Ed.* **2008**, *47*, 654–670. [[CrossRef](#)]
74. Wang, C.; Li, Z.; Sun, P.; Pei, H.; Yin, X. Preparation and Properties of Covalently Crosslinked Polybenzimidazole High Temperature Proton Exchange Membranes Doped with High Sulfonated Polyphosphazene. *J. Electrochem. Soc.* **2020**, *167*, 104517–104528. [[CrossRef](#)]
75. Rajabi, Z.; Javanbakht, M.; Hooshyari, K.; Badieli, A.; Adibi, M. High temperature composite membranes based on polybenzimidazole and dendrimer amines functionalized SBA-15 mesoporous silica for fuel cells. *New J. Chem.* **2020**, *44*, 5001–5018. [[CrossRef](#)]
76. Escorihuela, J.; García-Bernabé, A.; Montero, A.; Andrio, A.; Sahuquillo, O.; Giménez, E.; Compañ, V. Proton Conductivity through Polybenzimidazole Composite Membranes Containing Silica Nanofiber Mats. *Polymers* **2019**, *11*, 1182. [[CrossRef](#)] [[PubMed](#)]
77. Escorihuela, J.; Sahuquillo, O.; García-Bernabé, A.; Giménez, E.; Compañ, V. Phosphoric Acid Doped Polybenzimidazole (PBI)/Zeolitic Imidazolate Framework Composite Membranes with Significantly Enhanced Proton Conductivity under Low Humidity Conditions. *Nanomaterials* **2018**, *8*, 775. [[CrossRef](#)] [[PubMed](#)]
78. Abouzari-Lottf, E.; Zakeri, M.; Nasef, M.M.; Miyake, M.; Mozarmnia, P.; Bazilah, N.A.; Emelin, N.F.; Ahmad, A. Highly durable polybenzimidazole composite membranes with phosphonated graphene oxide for high temperature polymer electrolyte membrane fuel cells. *J. Power Sources* **2019**, *412*, 238–245. [[CrossRef](#)]
79. Quartarone, E.; Mustarelli, P. Polymer fuel cells based on polybenzimidazole/H₃PO₄. *Energy Environ. Sci.* **2012**, *5*, 6436–6444. [[CrossRef](#)]
80. Samms, S.R.; Wasmus, S.; Savinell, R.F. Thermal stability of proton conducting acid doped polybenzimidazole in simulated fuel cell environments. *J. Electrochem. Soc.* **1996**, *143*, 1225–1232. [[CrossRef](#)]
81. Yang, J.; Li, Q.; Cleemann, L.N.; Xu, C.; Jensen, J.O.; Pan, C.; Bjerrum, N.J.; He, R. Synthesis and properties of poly(aryl sulfone benzimidazole) and its copolymers for high temperature membrane electrolytes for fuel cells. *J. Mater. Chem.* **2012**, *22*, 11185–11195. [[CrossRef](#)]
82. Yang, J.; Aili, D.; Li, Q.; Xu, Y.; Liu, P.; Che, Q.; Jensen, J.O.; Bjerrum, N.J.; He, R. Benzimidazole grafted polybenzimidazoles for proton exchange membrane fuel cells. *Polym. Chem.* **2013**, *4*, 4768–4775. [[CrossRef](#)]
83. Li, J.; Li, X.; Zhao, Y.; Lu, W.; Shao, Z.; Yi, B. High-Temperature Proton-Exchange-Membrane Fuel Cells Using an Ether-Containing Polybenzimidazole Membrane as Electrolyte. *ChemSusChem* **2012**, *5*, 896–900. [[CrossRef](#)]
84. Berbera, M.R.; Nakashima, N. Bipyridine-based polybenzimidazole membranes with outstanding hydrogen fuel cell performance at high temperature and non-humidifying conditions. *J. Membr. Sci.* **2019**, *591*, 117354. [[CrossRef](#)]
85. Kang, Y.; Zou, J.; Sun, Z.; Wang, F.; Zhu, H.; Han, K.; Yang, W.; Song, H.; Meng, Q. Polybenzimidazole containing ether units as electrolyte for high temperature proton exchange membrane fuel cells. *Int. J. Hydrog. Energy* **2013**, *38*, 6494–6502. [[CrossRef](#)]
86. Ou, T.; Chen, H.; Hu, B.; Zheng, H.; Li, W.; Yi Wang, Y. A facile method of asymmetric ether-containing polybenzimidazole membrane for high temperature proton exchange membrane fuel cell. *Int. J. Hydrog. Energy* **2018**, *43*, 12337–12345. [[CrossRef](#)]
87. Bruma, M.; Fitch, J.W.; Cassidy, P.E. Hexafluoroisopropylidene-Containing Polymers for High-Performance Applications. *J. Macromol. Sci. Rev. Macromol. Chem. Phys.* **1996**, *C36*, 119–159. [[CrossRef](#)]

88. Qian, G.; Benicewicz, B.C. Synthesis and characterization of high molecular weight hexafluoroisopropylidene-containing polybenzimidazole for high-temperature polymer electrolyte membrane fuel cells. *J. Polym. Sci. Polym. Chem.* **2009**, *47*, 4064–4073. [[CrossRef](#)]
89. Yang, J.; Xu, Y.; Liu, P.; Gao, L.; Che, Q.; He, R. Epoxides cross-linked hexafluoropropylidene polybenzimidazole membranes for application as high temperature proton exchange membranes. *Electrochim. Acta* **2015**, *160*, 281–287. [[CrossRef](#)]
90. Kolb, H.C.; Finn, M.G.; Sharpless, K.B. Click Chemistry: Diverse Chemical Function from a Few Good Reactions. *Angew. Chem. Int. Ed.* **2001**, *40*, 2004–2021. [[CrossRef](#)]
91. Escorihuela, J.; Marcelis, A.T.M.; Zuilhof, H. Metal-Free Click Chemistry Reactions on Surfaces. *Adv. Mater. Interfaces* **2015**, *2*, 1500135. [[CrossRef](#)]
92. Sen, R.; Escorihuela, J.; Smulders, M.M.J.; Zuilhof, H. Use of Ambient Ionization High-Resolution Mass Spectrometry for the Kinetic Analysis of Organic Surface Reactions. *Langmuir* **2016**, *14*, 3412–3419. [[CrossRef](#)]
93. Lowe, A.B. Thiol-ene “click” reactions and recent applications in polymer and materials synthesis. *Polym. Chem.* **2010**, *1*, 17–36. [[CrossRef](#)]
94. Escorihuela, J.; Bañus, M.J.; Grijalvo, S.; Eritja, R.; Puchades, R.; Maquieira, A. Direct Covalent Attachment of DNA Microarrays by Rapid Thiol–Ene “Click” Chemistry. *Bioconjugate Chem.* **2014**, *25*, 618–627. [[CrossRef](#)]
95. Yao, B.; Mei, J.; Li, J.; Wang, J.; Wu, H.; Sun, J.Z.; Qin, A.; Tang, B.Z. Catalyst-Free Thiol–Yne Click Polymerization: A Powerful and Facile Tool for Preparation of Functional Poly(vinylene sulfide)s. *Macromolecules* **2014**, *47*, 1325–1333. [[CrossRef](#)]
96. Escorihuela, J.; Bañus, M.J.; Puchades, R.; Maquieira, A. Site-specific immobilization of DNA on silicon surfaces by using the thiol–yne reaction. *J. Mater. Chem. B* **2014**, *2*, 8510–8517. [[CrossRef](#)] [[PubMed](#)]
97. Sen, R.; Gahtory, D.; Escorihuela, J.; Firet, J.; Pujari, S.P.; Zuilhof, H. Approach Matters: The Kinetics of Interfacial Inverse-Electron Demand Diels–Alder Reactions. *Chem. Eur. J.* **2017**, *23*, 13015–13022. [[CrossRef](#)]
98. MacKenzie, D.A.; Sherratt, A.R.; Chigrinova, M.; Cheung, L.L.W.; Pezacki, J.P. Strain-promoted cycloadditions involving nitrones and alkynes—rapid tunable reactions for bioorthogonal labeling. *Curr. Opin. Chem. Biol.* **2014**, *21*, 81–88. [[CrossRef](#)] [[PubMed](#)]
99. Ning, X.; Temming, R.P.; Dommerholt, J.; Guo, J.; Ania, D.B.; Debets, M.F.; Wolfert, M.A.; Boons, G.-J.; van Delft, F.L. Protein modification by strain-promoted alkyne–nitron cycloaddition. *Angew. Chem. Int. Ed.* **2010**, *49*, 3065–3068. [[CrossRef](#)] [[PubMed](#)]
100. Sen, R.; Escorihuela, J.; van Delft, F.; Zuilhof, H. Rapid and Complete Surface Modification with Strain-Promoted Oxidation-Controlled Cyclooctyne-1,2-Quinone Cycloaddition (SPOCQ). *Angew. Chem. Int. Ed.* **2017**, *56*, 3299–3303. [[CrossRef](#)]
101. Escorihuela, J.; Das, A.; Looijen, W.J.E.; van Delft, F.L.; Aquino, A.J.A.; Lischka, H.; Zuilhof, H. Kinetics of the Strain-Promoted Oxidation-Controlled Cycloalkyne-1,2-quinone Cycloaddition: Experimental and Theoretical Studies. *J. Org. Chem.* **2018**, *83*, 244–252. [[CrossRef](#)]
102. Gahtory, D.; Sen, R.; Kuzmyn, A.R.; Escorihuela, J.; Zuilhof, H. Strain-Promoted Cycloaddition of Cyclopropenes with o-Quinones: A Rapid Click Reaction. *Angew. Chem. Int. Ed.* **2018**, *57*, 10118–10122. [[CrossRef](#)]
103. Leophairatana, P.; De Silva, C.C.; Koberstein, J.T. How good is CuAAC “click” chemistry for polymer coupling reactions? *J. Polym. Sci. A Polym. Chem.* **2018**, *56*, 75–84. [[CrossRef](#)]
104. Kumar, B.S.; Sana, B.; Unnikrishnan, G.; Jana, T.; Kumar, K.S.S. Polybenzimidazole co-polymers: Their synthesis, morphology and high temperature fuel cell membrane properties. *Polym. Chem.* **2020**, *11*, 1043–1054. [[CrossRef](#)]
105. Kulkarni, M.P.; Peckham, T.J.; Thomas, O.D.; Holdcroft, S. Synthesis of highly sulfonated polybenzimidazoles by direct copolymerization and grafting. *J. Polym. Sci. Part A Polym. Chem.* **2013**, *51*, 3654–3666. [[CrossRef](#)]
106. Aili, D.; Javakhishvili, I.; Han, J.; Jankova, K.; Pan, C.; Hvilsted, S.; Jensen, J.O.; Bjerrum, N.J.; Li, Q. Amino-Functional Polybenzimidazole Blends with Enhanced Phosphoric Acid Mediated Proton Conductivity as Fuel Cell Electrolytes. *Macromol. Chem. Phys.* **2016**, *217*, 1161–1168. [[CrossRef](#)]
107. Zhao, B.; Cheng, L.; Bei, Y.; Wang, S.; Cui, J.; Zhu, H.; Li, X.; Zhu, Q. Grafted polybenzimidazole copolymers bearing polyhedral oligosilsesquioxane pendant moieties. *Eur. Polym. J.* **2017**, *94*, 99–110. [[CrossRef](#)]
108. Lee, H.-S.; Roy, A.; Lane, O.; McGrath, J.E. Synthesis and characterization of poly(arylene ether sulfone)-b-polybenzimidazole copolymers for high temperature low humidity proton exchange membrane fuel cells. *Polymer* **2008**, *49*, 5387–5396. [[CrossRef](#)]

109. Kim, T.-H.; Kim, S.-K.; Lim, T.-W.; Lee, J.-C. Synthesis and properties of poly(aryl ether benzimidazole) copolymers for high-temperature fuel cell membranes. *J. Membr. Sci.* **2008**, *323*, 362–370. [[CrossRef](#)]
110. Pingitore, A.T.; Huang, F.; Qian, G.; Benicewicz, B.C. High-Temperature Polybenzimidazole Fuel Cell Membranes via a Sol-Gel Process Dispersions. *Chem. Mater.* **2005**, *17*, 5328–5333.
111. Mader, J.; Benicewicz, B.C. Synthesis and Properties of Random Copolymers of Functionalized Polybenzimidazoles for High Temperature Fuel Cells. *Fuel Cells* **2011**, *11*, 212–221. [[CrossRef](#)]
112. Seel, D.C.; Benicewicz, B.C. Polyphenylquinoxaline-Based ProtonExchange Membranes Synthesized via the PPA Process for High Temperature Fuel Cell Systems. *J. Membrane Sci.* **2012**, *405*, 57–67. [[CrossRef](#)]
113. Molleto, M.A.; Chen, X.; Ploehn, H.J.; Fishel, K.J.; Benicewicz, B.C. High Polymer Content 3,5-Pyridine Polybenzimidazole Copolymer Membranes with Improved Compressive Properties. *Fuel Cells* **2014**, *14*, 16–25. [[CrossRef](#)]
114. Molleto, M.; Chen, X.; Ploehn, H.J.; Benicewicz, B.C. High Polymer Content 2,5-Pyridine-Polybenzimidazole Copolymer Membranes with Improved Compressive Properties. *Fuel Cells* **2015**, *15*, 150–159. [[CrossRef](#)]
115. Schönberger, F.; Qian, G.; Benicewicz, B.C. Polybenzimidazole-based block copolymers: From monomers to membrane electrode assemblies for high temperature polymer electrolyte membrane fuel cells. *J. Polym. Sci. Part A Polym. Chem.* **2017**, *55*, 1831–1843. [[CrossRef](#)]
116. Maity, S.; Jana, T. Polybenzimidazole Block Copolymers for Fuel Cell: Synthesis and Studies of Block Length Effects on Nanophase Separation, Mechanical Properties, and Proton Conductivity of PEM. *ACS Appl. Mater. Interfaces* **2014**, *6*, 6851–6864. [[CrossRef](#)] [[PubMed](#)]
117. Chen, S.; Pan, H.; Chang, Z.; Jin, M.; Pu, H. Synthesis and study of pyridine-containing sulfonated polybenzimidazole multiblock copolymer for proton exchange membrane fuel cells. *Ionics* **2019**, *25*, 2255–2265. [[CrossRef](#)]
118. Yuan, Q.; Sun, G.-H.; Han, K.-F.; Yu, J.-H.; Zhu, H.; Wang, Z.-M. Copolymerization of 4-(3,4-diamino-phenoxy)-benzoic acid and 3,4-diaminobenzoic acid towards H₃PO₄-doped PBI membranes for proton conductor with better processability. *Eur. Polym. J.* **2016**, *85*, 175–186. [[CrossRef](#)]
119. Kim, S.-K.; Choi, S.-W.; Jeon, W.S.; Park, J.O.; Ko, T.; Chang, H.; Lee, J.-C. Cross-Linked Benzoxazine–Benzimidazole Copolymer Electrolyte Membranes for Fuel Cells at Elevated Temperature. *Macromolecules* **2012**, *45*, 1438–1446. [[CrossRef](#)]
120. Dechnik, J.; Gascon, J.; Doonan, C.J.; Janiak, C.; Sumby, C.J. Mixed-Matrix Membranes. *Angew. Chem. Int. Ed.* **2017**, *56*, 9292–9310. [[CrossRef](#)]
121. Devrim, Y.; Devrim, H.; Eroglu, I. Polybenzimidazole/SiO₂ hybrid membranes for high temperature proton exchange membrane fuel cells. *Int. J. Hydrog. Energy* **2016**, *41*, 10044–10052. [[CrossRef](#)]
122. Pinar, F.J.; Cañizares, P.; Rodrigo, M.A.; Úbeda, D.; Lobato, J. Long-term testing of a high-temperature proton exchange membrane fuel cell short stack operated with improved polybenzimidazole-based composite membranes. *J. Power Sources* **2015**, *274*, 177–185. [[CrossRef](#)]
123. Nawn, G.; Pace, G.; Lavina, S.; Vezz, K.; Ngro, E.; Bertasi, F.; Polizzi, S.; Di Noto, V. Nanocomposite membranes based on polybenzimidazole and ZrO₂ for high-temperature proton exchange membrane fuel cells. *ChemSusChem* **2015**, *8*, 1381–1393. [[CrossRef](#)]
124. Zhang, S.; Davaajargal, T.; Aiba, M.; Akasaka, S.; Ashizawa, M.; Tsuruoka, S.; Fugetsu, B.; Matsumoto, H. Enhancing water flux through semipermeable polybenzimidazole membranes by adding surfactant-treated CNTs. *J. Appl. Polym. Sci.* **2018**, *135*, 45875–45882. [[CrossRef](#)]
125. Xu, C.; Cao, Y.; Kumar, R.; Wu, X.; Wang, X.; Scott, K. A polybenzimidazole/sulfonated graphite oxide composite membrane for high temperature polymer electrolyte membrane fuel cells. *J. Mater. Chem.* **2011**, *21*, 11359–11364. [[CrossRef](#)]
126. Cai, Y.; Yue, Z.; Xu, S. A novel polybenzimidazole composite modified by sulfonated graphene oxide for high temperature proton exchange membrane fuel cells in anhydrous atmosphere. *J. Appl. Polym. Sci.* **2017**, *134*, 44986–44993. [[CrossRef](#)]
127. Gupta, C.; Maheshwari, P.H.; Dhakate, S.R. Development of multiwalled carbon nanotubes platinum nanocomposite as efficient PEM fuel cell catalyst. *Mater. Renew. Sustain. Energy* **2016**, *5*, 2.
128. Díaz, M.; Ortiz, A.; Ortiz, I. Progress in the use of ionic liquids as electrolyte membranes in fuel cells. *J. Membr. Sci.* **2014**, *469*, 379–396. [[CrossRef](#)]

129. Kallem, P.; Yanar, N.; Choi, H. Nanofiber-Based Proton Exchange Membranes: Development of Aligned Electrospun Nanofibers for Polymer Electrolyte Fuel Cell Applications. *ACS Sustain. Chem. Eng.* **2019**, *7*, 1808–1825. [[CrossRef](#)]
130. Lobato, J.; Cañizares, P.; Rodrigo, M.A.; Úbeda, D.; Pinar, F.J. A novel titanium PBI-based composite membrane for high temperature PEMFCs. *J. Memb. Sci.* **2011**, *369*, 105–111. [[CrossRef](#)]
131. Tahrim, A.A.; Amin, I.N.H.M. Advancement in Phosphoric Acid Doped Polybenzimidazole Membrane for High Temperature PEM Fuel Cells: A Review. *J Appl. Membr. Sci. Technol.* **2019**, *23*, 37–62. [[CrossRef](#)]
132. Pu, H.; Liu, L.; Chang, Z.; Yuan, J. Organic/inorganic composite membranes based on polybenzimidazole and nano-SiO₂. *Electrochim. Acta* **2009**, *54*, 7536–7541. [[CrossRef](#)]
133. Özdemir, Y.; Üregen, N.; Devrim, Y. Polybenzimidazole based nanocomposite membranes with enhanced proton conductivity for high temperature PEM fuel cells. *Int. J. Hydrog. Energy* **2017**, *42*, 2648–2657. [[CrossRef](#)]
134. Seo, K.; Seo, J.; Nam, K.H.; Han, H. Polybenzimidazole/Inorganic Composite Membrane With Advanced Performance for High Temperature Polymer Electrolyte Membrane Fuel Cells. *Polym. Compos.* **2015**, *38*, 87–95. [[CrossRef](#)]
135. Lysova, A.A.; Ponomarev, I.I.; Yaroslavtsev, A.B. Composite materials based on polybenzimidazole and inorganic oxides. *Solid State Ion.* **2011**, *188*, 132–134. [[CrossRef](#)]
136. Zhang, Q.; Liu, H.; Li, X.; Xu, R.; Zhong, J.; Chen, R.; Gu, X. Synthesis and Characterization of Polybenzimidazole/a-Zirconium Phosphate Composites as Proton Exchange Membrane. *Polym. Eng. Sci.* **2016**, *56*, 622–628. [[CrossRef](#)]
137. Lobato, J.; Cañizares, P.; Rodrigo, M.A.; Úbeda, D.; Pinar, F.J. Enhancement of the fuel cell performance of a high temperature proton exchange membrane fuel cell running with titanium composite polybenzimidazole-based membranes. *J. Power Sources* **2011**, *196*, 8265–8271. [[CrossRef](#)]
138. Shabanikia, A.; Javanbakht, M.; Amoli, H.S.; Hooshyari, K.; Enhessari, M. Novel nanocomposite membranes based on polybenzimidazole and Fe₂TiO₅ nanoparticles for proton exchange membrane fuel cells. *Ionics* **2015**, *21*, 2227–2236. [[CrossRef](#)]
139. Guanzhou, Q.; Jiang, T.; Hongxu, L.; Dianzuo, W. Functions and molecular structure of organic binders for iron ore pelletization. *Colloids Surf. A* **2003**, *224*, 11–22.
140. Mohammadi, G.; Jahanshahi, M.; Rahimpour, A. Fabrication and evaluation of Nafion nanocomposite membrane based on ZrO₂-TiO₂ binary nanoparticles as fuel cell MEA. *Int. J. Hydrog. Energy* **2013**, *38*, 9387–9394. [[CrossRef](#)]
141. He, R.; Li, Q.; Xiao, G.; Bjerrum, N.J. Proton conductivity of phosphoric acid doped polybenzimidazole and its composites with inorganic proton conductors. *J. Membran. Sci.* **2003**, *226*, 169–184. [[CrossRef](#)]
142. Di, S.; Yan, L.; Han, S.; Yue, B.; Feng, Q.; Xie, L.; Chen, J.; Zhang, D.; Sun, C. Enhancing the high-temperature proton conductivity of phosphoric acid doped poly(2,5-benzimidazole) by preblending boron phosphate nanoparticles to the raw materials. *J. Power Sources* **2012**, *211*, 161–168. [[CrossRef](#)]
143. Xu, C.; Wu, X.; Wang, X.; Mamlouk, M.; Scott, K. Composite membranes of polybenzimidazole and caesium-salts-of-heteropolyacids for intermediate temperature fuel cells. *J. Mater. Chem.* **2011**, *21*, 6014–6019. [[CrossRef](#)]
144. Hooshyari, K.; Javanbakht, M.; Shabanikia, A.; Enhessari, M. Fabrication BaZrO₃/PBI-based nanocomposite as a new proton conducting membrane for high temperature proton exchange membrane fuel cells. *J. Power Sources* **2015**, *276*, 62–72. [[CrossRef](#)]
145. Shabanikia, A.; Javanbakht, M.; Amoli, H.S.; Hooshyari, K.; Enhessari, M. Polybenzimidazole/strontium cerate nanocomposites with enhanced proton conductivity for proton exchange membrane fuel cells operating at high temperature. *Electrochim. Acta* **2015**, *154*, 370–378. [[CrossRef](#)]
146. Fuentes, I.; Andrio, A.; Teixidor, F.; Viñas, C.; Compañ, V. Enhanced conductivity of sodium versus lithium salts measured by impedance spectroscopy. Sodium Cobaltacarboranes Electrolytes Choice. *Phys. Chem. Chem. Phys.* **2017**, *19*, 15177–15186. [[CrossRef](#)] [[PubMed](#)]
147. Fuentes, I.; Andrio, A.; Garcia-Bernabé, A.; Escorihuela, J.; Viñas, C.; Teixidor, F.; Compañ, V. Structural and dielectric properties of cobaltacarborane composite polybenzimidazole membranes as solid polymer electrolytes at high temperature. *Phys. Chem. Chem. Phys.* **2018**, *20*, 10173–10184. [[CrossRef](#)] [[PubMed](#)]
148. Olvera-Mancilla, J.; Escorihuela, J.; Alexandrova, L.; Andrio, A.; García-Bernabé, A.; del Castillo, L.F.; Compañ, V. Effect of metallacarborane salt H[COSANE] doping on the performance properties of polybenzimidazole membranes for high temperature PEMFCs. *Soft Matter* **2020**, *16*. [[CrossRef](#)]

149. Stankovich, S.; Dikin, D.A.; Dommett, G.H.B.; Kohlhaas, K.M.; Zimmey, E.J.; Stach, E.A.; Piner, R.D.; Nguyen, S.-B.T.; Ruoff, S.R. Graphene-based composite materials. *Nature* **2006**, *442*, 282–286. [[CrossRef](#)] [[PubMed](#)]
150. Chee, W.K.; Lim, H.N.; Huang, N.M.; Harrison, I. Nanocomposites of Graphene/Polymers: A Review. *RSC Adv.* **2015**, *5*, 68014–68051. [[CrossRef](#)]
151. Xu, C.; Liu, X.; Cheng, J.; Scott, K. A polybenzimidazole/ionic-liquid-graphite-oxide composite membrane for high temperature polymer electrolyte membrane fuel cells. *J. Power Sources* **2015**, *274*, 922–927. [[CrossRef](#)]
152. Chen, D.; Tang, L.; Li, J. Graphene-based materials in electrochemistry. *Chem. Soc. Rev.* **2010**, *39*, 3157–3180. [[CrossRef](#)]
153. Yang, Y.-H.; Bolling, L.; Priolo, M.A.; Grunlan, J.C. Super gas barrier and selectivity of graphene oxide-polymer multilayer thin films. *Adv. Mater.* **2013**, *25*, 503–508. [[CrossRef](#)]
154. Thebo, K.H.; Qian, X.; Zhang, Q.; Chen, L.; Cheng, H.-M.; Ren, W. Highly stable graphene-oxide-based membranes with superior permeability. *Nat. Commun.* **2018**, *9*, 1486–1493. [[CrossRef](#)]
155. Ma, M.; Guo, L.; Anderson, D.G.; Langer, R. Bio-inspired polymer composite actuator and generator driven by water gradients. *Science* **2013**, *339*, 186–189. [[CrossRef](#)] [[PubMed](#)]
156. Chee, W.K.; Lim, H.N.; Harrison, I.; Chong, K.F.; Zainal, Z.; Ng, C.H.; Huang, N.M. Performance of flexible and binderless polypyrrole/graphene oxide/zinc oxide supercapacitor electrode in a symmetrical two-electrode configuration. *Electrochim. Acta* **2015**, *157*, 88–94.
157. Cao, J.; Chen, C.; Zhao, Q.; Zhang, N.; Lu, Q.; Wang, X.; Niu, Z.; Chen, J. A flexible nanostructured paper of a reduced graphene oxide–sulfur composite for high-performance lithium–sulfur batteries with unconventional configurations. *Adv. Mater.* **2016**, *28*, 9629–9636. [[CrossRef](#)] [[PubMed](#)]
158. Kim, K.S.; Zhao, Y.; Jang, H.; Lee, S.Y.; Kim, J.M.; Kim, K.S.; Ahn, J.-H.; Kim, P.; Choi, J.-Y.; Hong, B.H. Large-scale pattern growth of graphene films for stretchable transparent electrodes. *Nature* **2009**, *457*, 706–710. [[CrossRef](#)] [[PubMed](#)]
159. Yang, J.; Liu, C.; Gao, L.; Wang, J.; Xu, Y.; He, R. Novel composite membranes of triazole modified graphene oxide and polybenzimidazole for high temperature polymer electrolyte membrane fuel cell applications. *RSC Adv.* **2015**, *5*, 101049–101054. [[CrossRef](#)]
160. Adeli, M.; Soleyman, R.; Beiranvand, Z.; Madani, F. Carbon nanotubes in cancer therapy. *Chem. Soc. Rev.* **2013**, *42*, 5231–5256. [[CrossRef](#)]
161. Saito, N.; Haniu, H.; Usui, Y.; Aoki, K.; Hara, K.; Takashi, S.; Shimizu, M.; Narita, N.; Okamoto, M.; Kobayashi, S.; et al. Safe Clinical Use of Carbon Nanotubes as Innovative Biomaterials. *Chem. Rev.* **2014**, *114*, 6040–6079. [[CrossRef](#)]
162. Rajabi, M.; Mahanpoor, K.; Moradi, O. Removal of dye molecules from aqueous solution by carbon nanotubes and carbon nanotube functional groups: Critical review. *RSC Adv.* **2017**, *7*, 47083–47090. [[CrossRef](#)]
163. Yan, Y.; Miao, J.; Yang, Z.; Xiao, F.X.; Yang, H.B.; Liu, B.; Yang, Y. Carbon nanotube catalysts: Recent advances in synthesis, characterization and applications. *Chem. Soc. Rev.* **2015**, *44*, 3295–3346. [[CrossRef](#)]
164. Hu, L.; Hecht, D.S.; Grüner, G. Carbon Nanotube Thin Films: Fabrication, Properties, and Applications. *Chem. Rev.* **2010**, *110*, 5790–5844. [[CrossRef](#)]
165. Che, Y.; Chen, H.; Gui, H.; Liu, J.; Liu, B.; Zhou, C. Review of carbon nanotube nanoelectronics and macroelectronics. *Semicond. Sci. Technol.* **2014**, *29*, 073001–073017. [[CrossRef](#)]
166. Dillon, A.C. Carbon Nanotubes for Photoconversion and Electrical Energy Storage. *Chem. Rev.* **2010**, *110*, 6856–6872. [[CrossRef](#)] [[PubMed](#)]
167. Wang, L.; Liu, H.; Konik, R.M.; Misewich, J.A.; Wong, S.S. Carbon nanotube-based heterostructures for solar energy applications. *Chem. Soc. Rev.* **2013**, *42*, 8134–8156. [[CrossRef](#)] [[PubMed](#)]
168. Yu, L.P.; Shearer, C.; Shapter, J. Recent Development of Carbon Nanotube Transparent Conductive Films. *Chem. Rev.* **2016**, *116*, 13413–13453. [[CrossRef](#)] [[PubMed](#)]
169. Valitova, I.; Amato, M.; Mahvash, F.; Cantele, G.; Maffucci, A.; Santato, C.; Martel, R.; Ciccoira, F. Carbon nanotube electrodes in organic transistors. *Nanoscale* **2013**, *5*, 4638–4646. [[CrossRef](#)] [[PubMed](#)]
170. Cao, Z.; Wei, B.Q. A perspective: Carbon nanotube macro-films for energy storage. *Energy Environ. Sci.* **2013**, *6*, 3183–3201. [[CrossRef](#)]
171. De Volder, M.F.L.; Tawfick, S.H.; Baughman, R.H.; Hart, A.J. Carbon nanotubes: Present and future commercial applications. *Science* **2013**, *339*, 535–539. [[CrossRef](#)]

172. Zadehnazari, A.; Takassi, M.A. Synthesis of modified multi-walled carbon nanotube poly(benzimidazole-imide) composites: Assessment of morphological and thermomechanical properties. *Compos. Interfaces* **2016**, *23*, 909–924. [[CrossRef](#)]
173. Chang, C.M.; Liu, Y.L. Functionalization of multi-walled carbon nanotubes with non-reactive polymers through an ozone-mediated process for the preparation of a wide range of high performance polymer/carbon nanotube composites. *Carbon* **2010**, *48*, 1289–1297. [[CrossRef](#)]
174. Suryani; Chang, C.M.; Liu, Y.-L.; Lee, Y.M. Polybenzimidazole membranes modified with polyelectrolyte-functionalized multiwalled carbon nanotubes for proton exchange membrane fuel cells. *J. Mater. Chem.* **2011**, *21*, 7480–7486. [[CrossRef](#)]
175. Kannan, R.; Kagalwala, H.N.; Chaudhari, H.D.; Kharul, U.K.; Kurungot, S.; Pillai, V.K. Improved performance of phosphonated carbon nanotube–polybenzimidazole composite membranes in proton exchange membrane fuel cells. *J. Mater. Chem.* **2011**, *21*, 7223–7231. [[CrossRef](#)]
176. Jheng, L.C.; Huang, C.Y.; Hsu, S.L.C. Sulfonated MWNT and imidazole functionalized MWNT/polybenzimidazole composite membranes for high-temperature proton exchange membrane fuel cells. *Int. J. Hydrog. Energy* **2013**, *38*, 1524–1534. [[CrossRef](#)]
177. Du, C.Y.; Zhao, T.S.; Liang, X.Z. Sulfonation of carbon-nanotube supported platinum catalysts for polymer electrolyte fuel cells. *J. Power Sources* **2008**, *176*, 9–15. [[CrossRef](#)]
178. Park, M.J.; Lee, J.K.; Lee, B.S.; Lee, Y.W.; Choi, I.S.; Lee, S. Covalent Modification of Multiwalled Carbon Nanotubes with Imidazolium-Based Ionic Liquids: Effect of Anions on Solubility. *Chem. Mater.* **2006**, *18*, 1546–1551.
179. Guerrero Moreno, N.; Gervasio, D.; Godínez García, A.; Pérez Robles, J.F. Polybenzimidazole-multiwall carbon nanotubes composite membranes for polymer electrolyte membrane fuel cells. *J. Power Sources* **2015**, *300*, 229–237. [[CrossRef](#)]
180. Escorihuela, J.; Narducci, R.; Compañ, V.; Costantino, F. Proton conductivity of composite polyelectrolyte membranes with metal-organic frameworks for fuel cell applications. *Adv. Mater. Interfaces* **2019**, *6*, 1801146. [[CrossRef](#)]
181. Ramaswamy, P.; Wong, N.E.; Gelfand, B.S.; Shimizu, G.K.H. Straightforward Loading of Imidazole Molecules into Metal–Organic Framework for High Proton Conduction. *J. Am. Chem. Soc.* **2015**, *137*, 7640–7643. [[CrossRef](#)] [[PubMed](#)]
182. Diercks, C.S.; Yaghi, O.M. The Atom, the Molecule, and the Covalent Organic Framework. *Science* **2017**, *355*, 923. [[CrossRef](#)]
183. Lim, D.-W.; Kitagawa, H. Proton Transport in Metal–Organic Frameworks. *Chem. Rev.* **2020**. [[CrossRef](#)]
184. Eddaoudi, M.; Kim, J.; Rosi, N.; Vodak, D.; Wachter, J.; O’Keeffe, M.; Yaghi, O.M. Systematic Design of Pore Size and Functionality in Isoreticular MOFs and Their Application in Methane Storage. *Science* **2002**, *295*, 469–472. [[CrossRef](#)]
185. Huang, Y.-B.; Liang, J.; Wang, X.-S.; Cao, R. Multifunctional metal–organic framework catalysts: Synergistic catalysis and tandem reactions. *Chem. Soc. Rev.* **2017**, *46*, 126–157. [[CrossRef](#)]
186. Banerjee, D.; Cairns, A.J.; Liu, J.; Motkuri, R.K.; Nune, S.K.; Fernandez, C.A.; Krishna, R.; Strachan, D.M.; Thallapally, P.K. Potential of Metal–Organic Frameworks for Separation of Xenon and Krypton. *Acc. Chem. Res.* **2015**, *48*, 211–219. [[CrossRef](#)]
187. Wen, X.; Zhang, Q.; Guan, J. Applications of metal–organic framework-derived materials in fuel cells and metal-air batteries. *Coord. Chem. Rev.* **2020**, *409*, 213214. [[CrossRef](#)]
188. Shi, G.M.; Yang, T.; Chung, T.S. Polybenzimidazole (PBI)/zeolitic imidazolate frameworks (ZIF-8) mixed matrix membranes for pervaporation dehydration of alcohols. *J. Memb. Sci.* **2012**, *415–416*, 577–586. [[CrossRef](#)]
189. Fei, F.; Cseri, L.; Szekely, G.; Blanford, C.F. Robust Covalently Cross-linked Polybenzimidazole/Graphene Oxide Membranes for High-Flux Organic Solvent Nanofiltration. *ACS Appl. Mater. Interfaces* **2018**, *10*, 16140–16147. [[CrossRef](#)] [[PubMed](#)]
190. Zhang, Z.; Nguyen, H.T.H.; Miller, S.A.; Ploskonka, A.M.; DeCoste, J.B.; Cohen, S.M. Polymer–Metal–Organic Frameworks (polyMOFs) as Water Tolerant Materials for Selective Carbon Dioxide Separations. *J. Am. Chem. Soc.* **2016**, *138*, 920–925. [[CrossRef](#)] [[PubMed](#)]
191. DeCoste, J.B.; Denny, M.S., Jr.; Peterson, G.W.; Mahle, J.J.; Cohen, S.M. Enhanced aging properties of HKUST-1 in hydrophobic mixed-matrix membranes for ammonia adsorption. *Chem. Sci.* **2016**, *7*, 2711–2716. [[CrossRef](#)] [[PubMed](#)]

192. Didaskalou, C.; Kupai, J.; Cseri, L.; Barabas, J.; Vass, E.; Holtzl, T.; Szekely, G. Membrane-Grafted Asymmetric Organocatalyst for an Integrated Synthesis–Separation Platform. *ACS Catal.* **2018**, *8*, 7430–7438. [[CrossRef](#)]
193. Sun, Y.; Sun, L.; Feng, D.; Zhou, H.-C. An In Situ One-Pot Synthetic Approach Towards Multivariate Zirconium MOFs. *Angew. Chem. Int. Ed.* **2016**, *55*, 6471–6475. [[CrossRef](#)]
194. Donnadio, A.; Narducci, R.; Casciola, M.; Marmottini, F.; D’Amato, R.; Jazestani, M.; Chiniforoshan, H.; Costantino, F. Mixed Membrane Matrices Based on Nafion/UiO-66/SO₃H-UiO-66 Nano-MOFs: Revealing the Effect of Crystal Size, Sulfonation, and Filler Loading on the Mechanical and Conductivity Properties. *ACS Appl. Mater. Interfaces* **2017**, *9*, 42239–42246. [[CrossRef](#)]
195. Rao, Z.; Feng, K.; Tang, B.; Wu, P. Construction of well interconnected metal-organic framework structure for effectively promoting proton conductivity of proton exchange membrane. *J. Membr. Sci.* **2017**, *533*, 160–170. [[CrossRef](#)]
196. Cai, K.; Sun, F.; Liang, X.; Liu, C.; Zhao, N.; Zou, X.; Zhu, G. An acid-stable hexaphosphate ester based metal–organic framework and its polymer composite as proton exchange membrane. *J. Mater. Chem. A* **2017**, *5*, 12943–12950. [[CrossRef](#)]
197. Tsai, C.H.; Wang, C.C.; Chang, C.Y.; Lin, C.H.; Chen-Yang, Y.W. Enhancing performance of Nafion®-based PEMFC by 1-D channel metal-organic frameworks as PEM filler. *Int. J. Hydrog. Energy* **2014**, *39*, 15696–15705. [[CrossRef](#)]
198. Kim, H.J.; Talukdar, K.; Choi, S.J. Tuning of Nafion® by HKUST-1 as coordination network to enhance proton conductivity for fuel cell applications. *J. Nanopart. Res.* **2016**, *18*, 47. [[CrossRef](#)]
199. Sun, H.Z.; Tang, B.B.; Wu, P.Y. Rational Design of S-UiO-66@GO Hybrid Nanosheets for Proton Exchange Membranes with Significantly Enhanced Transport Performance. *ACS Appl. Mater. Interfaces* **2017**, *9*, 26077–26087. [[CrossRef](#)] [[PubMed](#)]
200. Han, R.; Wu, P.Y. Composite Proton-Exchange Membrane with Highly Improved Proton Conductivity Prepared by in Situ Crystallization of Porous Organic Cage. *ACS Appl. Mater. Interfaces* **2018**, *10*, 18351–18358. [[CrossRef](#)]
201. Patel, H.A.; Mansor, N.; Gadipelli, S.; Brett, D.J.L.; Guo, Z. Superacidity in Nafion/MOF Hybrid Membranes Retains Water at Low Humidity to Enhance Proton Conduction for Fuel Cells. *ACS Appl. Mater. Interfaces* **2016**, *8*, 30687–30691. [[CrossRef](#)]
202. Li, Z.; He, G.W.; Zhao, Y.N.; Cao, Y.; Wu, H.; Li, Y.F.; Jiang, Z.Y. Enhanced proton conductivity of proton exchange membranes by incorporating sulfonated metal-organic frameworks. *J. Power Sources* **2014**, *262*, 372–379. [[CrossRef](#)]
203. Wu, B.; Pan, J.; Ge, L.; Wu, L.; Wang, H.; Xu, T. Oriented MOF-polymer Composite Nanofiber Membranes for High Proton Conductivity at High Temperature and Anhydrous Condition. *Sci. Rep.* **2014**, *4*, 4334. [[CrossRef](#)]
204. Ru, C.; Li, Z.; Zhao, C.; Duan, Y.; Zhuang, Z.; Bu, F.; Na, H. Enhanced Proton Conductivity of Sulfonated Hybrid Poly(arylene ether ketone) Membranes by Incorporating an Amino–Sulfo Bifunctionalized Metal–Organic Framework for Direct Methanol Fuel Cells. *ACS Appl. Mater. Interfaces* **2018**, *10*, 7963–7973. [[CrossRef](#)]
205. Zhang, B.; Cao, Y.; Li, Z.; Wu, H.; Yin, Y.H.; Cao, L.; He, X.Y.; Jiang, Z.Y. Proton exchange nanohybrid membranes with high phosphotungstic acid loading within metal-organic frameworks for PEMFC applications. *Electrochim. Acta* **2017**, *240*, 186–194. [[CrossRef](#)]
206. Ahmadian-Alam, L.; Mahdavi, H. A novel polysulfone-based ternary nanocomposite membrane consisting of metal-organic framework and silica nanoparticles: As proton exchange membrane for polymer electrolyte fuel cells. *Renew. Energy* **2018**, *126*, 630. [[CrossRef](#)]
207. Vega, J.; Andrio, A.; Lemus, A.A.; del Castillo, L.F.; Compañ, V. Conductivity study of Zeolitic Imidazolate Frameworks, Tetrabutylammonium hydroxide doped with Zeolitic Imidazolate Frameworks, and mixed matrix membranes of Polyetherimide/Tetrabutylammonium hydroxide doped with Zeolitic Imidazolate Frameworks for proton conducting applications. *Electrochim. Acta* **2017**, *258*, 153–166.
208. Wu, B.; Lin, X.; Ge, L.; Wu, L.; Xu, T. A novel route for preparing highly proton conductive membrane materials with metal-organic frameworks. *Chem. Commun.* **2013**, *49*, 143–145.
209. Fadzallah, I.A.; Majid, S.R.; Careem, M.A.; Arof, A.K. A study on ionic interactions in chitosan–oxalic acid polymer electrolyte membranes. *J. Membr. Sci.* **2014**, *463*, 65–72.

210. Erkartal, M.; Usta, H.; Citir, M.; Sen, U. Proton conducting poly(vinyl alcohol) (PVA)/poly(2-acrylamido-2-methylpropane sulfonic acid) (PAMPS)/zeolitic imidazolate framework (ZIF) ternary composite membrane. *J. Membr. Sci.* **2016**, *499*, 156–163.
211. Liang, X.; Zhang, F.; Feng, W.; Zou, X.; Zhao, C.; Na, H.; Liu, C.; Sun, F.; Zhu, G. From metal–organic framework (MOF) to MOF–polymer composite membrane: Enhancement of low-humidity proton conductivity. *Chem. Sci.* **2013**, *4*, 983–992.
212. Park, K.S.; Ni, Z.; Cote, A.P.; Choi, J.Y.; Huang, R.; Uribe-Romo, F.J.; Chae, H.K.; O’Keeffe, M.; Yaghi, O.M. Exceptional chemical and thermal stability of zeolitic imidazolate frameworks. *Proc. Natl. Acad. Sci. USA* **2006**, *103*, 10186–10191. [[CrossRef](#)] [[PubMed](#)]
213. Erkartal, M.; Erkilic, U.; Tam, B.; Usta, H.; Yazaydin, O.; Hupp, J.T.; Farha, O.K.; Sen, U. From 2-methylimidazole to 1,2,3-triazole: A topological transformation of ZIF-8 and ZIF-67 by post-synthetic modification. *Chem. Commun.* **2017**, *53*, 2028–2031. [[CrossRef](#)] [[PubMed](#)]
214. Plechkova, N.V.; Seddon, K.R. Applications of ionic liquids in the chemical industry. *Chem. Soc. Rev.* **2008**, *37*, 123–150. [[CrossRef](#)] [[PubMed](#)]
215. Earle, M.J.; Seddon, K.R. Ionic liquids. Green Solvents Future. *Pure Appl. Chem.* **2000**, *72*, 1391–1398. [[CrossRef](#)]
216. Dai, C.; Zhang, J.; Huang, C.; Lei, Z. Ionic liquids in selective oxidation: Catalysts and solvents. *Chem. Rev.* **2017**, *117*, 6929–6983. [[CrossRef](#)] [[PubMed](#)]
217. González, L.; Escorihuela, J.; Altava, B.; Burguete, M.I.; Luis, S.V. Chiral room temperature ionic liquids as enantioselective promoters for the asymmetric aldol reaction. *Eur. J. Org. Chem.* **2014**, 5356–5363. [[CrossRef](#)]
218. Chen, D.; Ying, W.; Guo, Y.; Ying, Y.; Peng, X. Enhanced Gas Separation through Nanoconfined Ionic Liquid in Laminated MoS₂ Membrane. *ACS Appl. Mater. Interfaces* **2017**, *9*, 44251–44257. [[CrossRef](#)]
219. González-Mendoza, L.; Escorihuela, J.; Altava, B.; Burguete, M.I.; Luis, S.V. Application of optically active chiral bis-(imidazolium) salts as potential receptors of chiral dicarboxylate salts of biological relevance. *Org. Biomol. Chem.* **2015**, *13*, 5450–5459. [[CrossRef](#)]
220. Valls, A.; Altava, B.; Burguete, M.I.; Escorihuela, J.; Martí-Centelles, V.; Luis, S.V. Supramolecularly assisted synthesis of chiral tripodal imidazolium compounds. *Org. Chem. Front.* **2019**, *6*, 1214–1225. [[CrossRef](#)]
221. González-Mendoza, L.; Altava, B.; Burguete, M.I.; Escorihuela, J.; Hernando, E.; Luis, S.V.; Quesada, R.; Vicent, C. Bis(imidazolium) salts derived from amino acids as receptors and transport agents for chloride anions. *RSC Adv.* **2015**, *5*, 34415–34423. [[CrossRef](#)]
222. Marrucho, I.M.; Branco, L.C.; Rebelo, L.P.N. Ionic Liquids in Pharmaceutical Applications. *Annu. Rev. Chem. Biomol. Eng.* **2014**, *5*, 527–546. [[CrossRef](#)] [[PubMed](#)]
223. Egorova, K.S.; Gordeev, E.G.; Ananikov, V.P. Biological activity of ionic liquids and their application in pharmaceuticals and medicine. *Chem. Rev.* **2017**, *117*, 7132–7189. [[CrossRef](#)] [[PubMed](#)]
224. Ye, Y.-S.; Ricka, J.; Hwang, B.-J. Ionic liquid polymer electrolytes. *J. Mater. Chem. A* **2013**, *1*, 2719–2743. [[CrossRef](#)]
225. Wang, J.T.-W.; Hsu, S.L.-C. Enhanced high-temperature polymer electrolyte membrane for fuel cells based on polybenzimidazole and ionic liquids. *Electrochim. Acta* **2011**, *56*, 2842–2846. [[CrossRef](#)]
226. Van de Ven, E.; Chairuna, A.; Merle, G.; Pacheco Benito, S.; Borneman, S.; Nijmeijer, K. Ionic liquid doped polybenzimidazole membranes for high temperature Proton Exchange Membrane fuel cell applications. *J. Power Sources* **2013**, *222*, 202–209. [[CrossRef](#)]
227. Escorihuela, J.; García-Bernabé, A.; Montero, A.; Sahuquillo, O.; Giménez, E.; Compañ, V. Ionic Liquid Composite Polybenzimidazol Membranes for High Temperature PEMFC Applications. *Polymers* **2019**, *11*, 732. [[CrossRef](#)]
228. Compañ, V.; Escorihuela, J.; Olvera, J.; García-Bernabé, A.; Andrio, A. Influence of the anion on diffusivity and mobility of ionic liquids composite polybenzimidazol membranes. *Electrochim. Acta* **2020**, *354*, 136666. [[CrossRef](#)]
229. Liu, S.; Zhou, L.; Wang, P.; Zhang, F.; Yu, S.; Shao, Z.; Yi, B. Ionic-Liquid-Based Proton Conducting Membranes for Anhydrous H₂/Cl₂ Fuel-Cell Applications. *ACS Appl. Mater. Interfaces* **2014**, *6*, 3195–3200. [[CrossRef](#)]
230. Song, X.; Ding, L.; Wang, L.; He, M.; Han, X. Polybenzimidazole membranes embedded with ionic liquids for use in high proton selectivity vanadium redox flow batteries. *Electrochim. Acta* **2019**, *295*, 1034–1043. [[CrossRef](#)]

231. Liao, Y.; Loh, C.-H.; Tian, M.; Wang, R.; Fane, A.G. Progress in electrospun polymeric nanofibrous membranes for water treatment: Fabrication, modification and applications. *Prog. Polym. Sci.* **2018**, *77*, 69–94. [CrossRef]
232. Lee, C.; Jo, S.M.; Choi, J.; Baek, K.-Y.; Truong, Y.B.; Kyratzis, I.L.; Shul, Y.-G. SiO₂/sulfonated poly ether ether ketone (SPEEK) composite nanofiber mat supported proton exchange membranes for fuel cells. *J. Mater. Sci.* **2013**, *48*, 3665–3671. [CrossRef]
233. Reyes-Rodriguez, J.L.; Escorihuela, J.; García-Bernabé, A.; Giménez, E.; Solorza-Feria, O.; Compañ, V. Proton conducting electrospun sulfonated polyether ether ketone graphene oxide composite membranes. *RSC Adv.* **2017**, *7*, 53481–53491. [CrossRef]
234. Yu, D.M.; Yoon, S.; Kim, T.-H.; Lee, J.Y.; Lee, J.; Hong, Y.T. Properties of sulfonated poly(arylene ether sulfone)/electrospun nonwoven polyacrylonitrile composite membrane for proton exchange membrane fuel cells. *J. Membr. Sci.* **2013**, *446*, 212–219. [CrossRef]
235. Laforgue, A.; Robitaille, L.; Mokrini, A.; Aji, A. Fabrication and Characterization of Ionic Conducting Nanofibers. *Macromol. Mater. Eng.* **2007**, *292*, 1229–1236. [CrossRef]
236. Wang, L.; Zhu, J.; Zheng, J.; Zhang, S.; Dou, L. Nanofiber mats electrospun from composite proton exchange membranes prepared from poly(aryl ether sulfone)s with pendant sulfonated aliphatic side chains. *RSC Adv.* **2014**, *4*, 25195–25200. [CrossRef]
237. Dong, B.; Gwee, L.; Salas-de la Cruz, D.; Winey, K.I.; Yossef, A.; Elabd, Y.A. Super Proton Conductive High-Purity Nafion Nanofibers. *Nano Lett.* **2010**, *10*, 3785–3790. [CrossRef]
238. Li, H.-Y.; Liu, Y.-L. Polyelectrolyte composite membranes of polybenzimidazole and crosslinked polybenzimidazole-polybenzoxazine electrospun nanofibers for proton exchange membrane fuel cells. *J. Mater. Chem. A* **2013**, *1*, 1171–1178. [CrossRef]
239. Muthuraja, P.; Prakash, S.; Manisankar, P. Stable nanofibrous poly(aryl sulfone ether benzimidazole) membrane with high conductivity for high temperature PEM fuel cells. *Solid State Ion.* **2018**, *317*, 201–209. [CrossRef]
240. Jahangiri, S.; Aravi, I.; Isikel Sanli, L.; Menciloglu, Y.Z.; Özden-Yenigün, E. Fabrication and optimization of proton conductive polybenzimidazole electrospun nanofiber membranes. *Polym. Adv. Tech.* **2018**, *29*, 594–602. [CrossRef]
241. Escorihuela, J.; Pujari, S.P.; Zuilhof, H. Organic monolayers by B(C₆F₅)₃-catalyzed siloxanation of oxidized silicon surfaces. *Langmuir* **2017**, *33*, 2185–2193. [CrossRef]
242. Escorihuela, J.; Zuilhof, H. Rapid surface functionalization of hydrogen-terminated silicon by alkyl silanols. *J. Am. Chem. Soc.* **2017**, *139*, 5870–5876. [CrossRef] [PubMed]
243. Escorihuela, J.; Bañuls, M.J.; García-Castelló, J.; Toccafondo, V.; García-Rupérez, J.; Puchades, R.; Maquieira, A. Chemical silicon surface modification and bioreceptor attachment to develop competitive integrated photonic biosensors. *Anal. Bioanal. Chem.* **2012**, *404*, 2831–2840. [CrossRef] [PubMed]
244. Available online: <https://www.mordorintelligence.com/industry-reports/global-polymer-electrolyte-membrane-pem-fuel-cells-market-industry> (accessed on 10 July 2020).
245. Available online: <https://www.advent.energy/products-high-temperature-meas/> (accessed on 20 July 2020).



© 2020 by the authors. Licensee MDPI, Basel, Switzerland. This article is an open access article distributed under the terms and conditions of the Creative Commons Attribution (CC BY) license (<http://creativecommons.org/licenses/by/4.0/>).